UDC 546.26-162:539.89

V. V. Brazhkin, A. G. Lyapin (Troitsk, Russia)

Hard and superhard carbon phases synthesised from fullerites under pressure

A review has been presented on the structural and mechanical properties of hard carbon phases synthesized from fullerite C_{60} under pressure. The density and nanostructure have been recognized as the key parameters defining the mechanical properties of hard carbon phases. By suggesting a version of the transitional high-pressure diagram of C_{60} (developed up to 20 GPa), the three areas of the formation of hard carbon phases have been highlighted. The corresponding phases of superhard carbon are (1) disordered sp^2-type atomic structures at moderate pressures and high temperatures (> 1100 K), (2) three-dimensionally polymerized C_{60} structures at moderate temperatures and high pressures (> 8 GPa), and (3) sp^3-based amorphous and nanocomposite phases at high pressures and temperatures. First region can be in turn separated into 2 subparts with different peculiarities of sp^2 structures and properties: low pressure part (0.1–2 GPa) and high-pressure part (2–8 GPa). Temperature can be recognized as a factor responsible for the formation of nanostructures by the partial destruction of molecular phases, whereas pressure is a factor responsible for stimulating the formation of rigid polymerized structures consisting of covalently bonded C_{60} molecules, whereas the combination of both factors leads to the formation of atomic-based phases with dominating sp^3 bonding.

Keywords*: carbon, diamond, fullerite C_{60}, nanostructure, polymerization, superhard phases.*

1. INTRODUCTION

Superhard materials are of great importance in the modern industry and this stimulates both scientific interest in such materials and regular attempts to synthesize new superhard substances with unusual properties. A fundamental problem, whose solution reflects the depth of our insight into the interrelation between the structure of a substance, interatomic forces, and its physical properties, exists in the physics of superhard materials. It is necessary to highlight clear relations between mechanical properties of substances, their elastic moduli, atomic or electron density, and real structures of different space scales, including defect states and material morphology. Carbon materials attract considerable interest of researchers because carbon–carbon bonds are among the shortest and strongest ones and therefore, the majority of carbon phases should have an advantageous combination of high mechanical characteristics and low density. Carbon atoms can occupy the two-, three-, or four-fold (*sp*-, sp^2-, and sp^3-hybridized, respectively) sites in solids. Due to this diversity of chemical bonding in solid carbon, carbon allotropes are combined into a great family of materials with the bonding type varying from zero-dimensional (Van der Waals cluster solids) to three-dimensional (3D). The reason for the occurrence of various types of chemical bonds between carbon atoms is related to the closeness of the bond energies per atom for various carbon states. In turn, this is due to the small size of the inner electron shell of a carbon atom and relatively close energies of σ- and π-bonding [1].

Among the carbon phases, diamond and diamond-containing materials are attracting special attention of researchers and technologists because of the unique intrinsic mechanical properties of such materials. Artificial diamond is ordinarily synthesized from graphite, which is stable under normal conditions. At the same time from the standpoint of fundamental investigations and for technological applications, it is of enormous interest to study the possibility for synthesizing diamond and other hard carbon modifications from metastable carbon phases. In this respect, the production of a new, highly metastable, ordered phase of carbon, fullerite C_{60}, in macroscopic quantities [2] has led to new possibilities for synthesizing new hard carbon materials via non-equilibrium transformations of C_{60} under pressure [3–5]. The thermodynamic relations provide an actual opportunity to influence the kinetics of transformations from the metastable fullerite C_{60} to stable phases, diamond and graphite, under high-pressure and high-temperature conditions.

The subject of the present review concerns carbon phases prepared from fullerite C_{60} by the pressure-temperature treatment. A large variety of all-carbon structures can be formed due to the covalent interaction between C_{60} molecules and the subsequent high-temperature atomic rearrangement under pressure. Among the pressure-synthesized C_{60}-based phases several ordered and disordered modifications have been clearly identified to date, including crystalline 1D and 2D C_{60} polymers [6–16], very hard graphite-type (sp^2-based) disordered phases [8, 14, 17–21], 3D polymers with a varying degree of polymerization [13, 22–37], diamond-like (sp^3-based) amorphous phases [26, 28, 37–39], and diamond–graphite nanocomposites [26, 28, 40–42]. Here we review our original data on mechanical properties of various carbon phases, pressure-synthesized from C_{60}, as well as the relevant results from the regular publications. The structural nature of the phases under discussion is considered in terms of the nonequilibrium transitional pressure–temperature diagram of C_{60}, where the types of transitions can be considered in terms of the bonding nature of involved parent and final phases. The data presented allow us to discuss the interplay between the bonding nature and the physical properties of covalent carbon compounds. The potential of pressure-synthesized C_{60}-based carbon materials is another issue of the current discussion. The main accent of this chapter is directed toward superhard materials prepared from C_{60}, whereas other topics concerning, e.g., structural, electronic, and optical properties of polymeric C_{60} phases can be found in the existing reviews [43–45].

The review is structured as follows. In Section 2 we discuss the problems of reliable measurements of hardness and elastic moduli. In Section 3 we consider the physical background of high elastic constants of superhard materials and the ways to get a “bridge” to “ideal” mechanical properties. In Section 4 we briefly present the experimental methods used in the original studies lying in the background of the current review. Section 5 is devoted to the general aspects of the transitional pressure–temperature phase diagram of C_{60}. In Section 6 we point out the areas in the transitional phase diagram of C_{60}, where one can obtain hard carbon phases and identify the role of external conditions in the formation of the hard carbon phases. In Section 7 we consider hard nanostructured carbon phases prepared at moderate pressures (0.1–1.5 GPa). The highest mechanical properties, observed for diamond-based nanocomposites among other phases produced from C_{60}, are considered in Section 8. The review of mechanical properties is presented in Section 9, where we also discuss their correlations with the structure and density. In Section 10 we focus on the influence of non-hydrostatic stresses on the anisotropic elasticity and

hardness. Finally, in the Conclusion (Section 11) we discuss the prospects for the application of hard carbon materials prepared from C_{60} under pressure.

2. HARDNESS AND MODULI MEASUREMENTS

Hardness is defined as "the resistance of a material to the imprinting or scratching" or, in particular, as "the property of materials to resist the penetration of other bodies into them". There are about 10 various quantitative and semi-quantitative definitions of the hardness and the corresponding scales. The Vickers method, according to which hardness is determined from the equation $H_V = P/S$, where P is the load on the pyramid and S is the area of the lateral surface of corresponding imprint on the sample studied, is most frequently used in physics for investigating mechanical properties of superhard materials. In the classical variant of the Vickers method, the imprint area is measured after the indentation. However, it is well known that after removing the load, a partial elastic recovery of the imprint takes place. Moreover, in the limit of very low loads, the indentation regime can be completely elastic, and after the load removal, there will be virtually no imprint. The method of nanoindentation, in which the penetration depth (and, consequently, the imprint area) is measured in the process of loading of the indenter as a function of the load value, has been developed recently and significantly extends the possibilities of experimenters. When the modern instruments for the nanoindentation with a continuous load increase are used, the loading curves contain information about both the elastic and plastic modes of the indentation.

The initial segment of the loading curve virtually contains information about elastic properties of a substance. In the limit of low loads, at the indentation by an absolutely hard cone of pyramid, the solution of the Hertz elastic contact problem yields [46]:

$$(P/S)_{\text{elast}} = \frac{E \operatorname{ctg} \phi}{2(1-\nu^2)},$$

where E is the Young modulus, ϕ is half the apex angle of the cone or pyramid and ν is the Poisson ratio. In the regime of the elastic mode of indentation, the $(P/S)_{\text{elast}}$ is at maximum on the whole loading curve. It is reasonable to introduce the concept of the limit of hardness for the ratio P/S. The real hardness, i.e. measured in the particular indentation experiment, can depend on the temperature, rate and time of loading, intergranular structure and texture of the sample, presence of defects, etc. The role of these factors is controlled by their influence on the character of plastic deformation and processes of the generation of defects determining the kinetics of plastic mass transfer. Temperature changes can result in replacing the brittle regime of indentation with the plastic one. For the majority of metals, such a transition takes place at temperatures considerably below room temperature. As a consequence, the hardness of the majority of metals under normal conditions is lower than the ideal hardness by a factor of several tens. For the majority of superhard materials, including diamond, the transition to the plastic regime of deformation occurs at temperatures substantially higher than room temperature. Comparing the hardness of various substances, one has to take into account the temperature of measurements. For example, diamond, being the hardest material at normal conditions, is less hard than the binary compound SiC at $T \approx 1400$ K, for diamond $H_V \approx 20$ GPa, whereas for SiC $H_V \approx 25$ GPa. In the plastic regime, the similarity law $P \propto S \propto d^2$ (d is the imprint size) is not fulfilled rigorously. The hardness–imprint size dependence can be described by simple

empirical relations, for example, by the Mayer classical law $P = Ad^n$, where A and n are constants and n usually assumes the values in the interval from 1.5 to 2, or by simple algebraic formulas of the $P = a_1 d + a_2 d^2$ type [47].

The value of the measured hardness can depend on the time characteristics of the experiment, because the indentation leads to rather complicated kinetics processes, including the generation of new defects, such as dislocations or twins and the plastic flow at the conditions of strong gradients of pressures and stresses. Summarizing, it can be inferred that the hardness depends on a great number of factors and, therefore, is not a well-defined and unambiguous characteristic.

It should be noted that the experimental study of elastic moduli of superhard materials is also a rather difficult task. Moreover, theoretical estimations often yield more accurate data in this respect than the experimental studies. For unambiguous measurements of the bulk and shear moduli, we need sufficiently large homogeneous samples, preferably as a large single crystals. Unfortunately, in most cases the samples to be studied are small, inhomogeneous, textured, etc. During an X-ray study of the compressibility (bulk modulus), the hydrostaticity of the pressure-transmitting medium is the most important and critical factor. Under the non-hydrostatic conditions it is easy to overestimate the bulk modulus value by several times. For example, 3D-polymers of fullerite C_{60} have the bulk modulus around 280 GPa [33], whereas wrong measurements, neglecting nonhydrostatic conditions of measurement, give the values 540 GPa (!) [48]. For the ultrasonic and Brillouin scattering study of elastic moduli, the isotropy and homogeneity of the sample are the key properties for correct determination of elastic characteristics. So, the neglecting of the texture for superhard amorphous carbon materials prepared from fullerite C_{60} leads to the overestimation of bulk modulus by 3 times! [49]. The whole set of experimental techniques, including high-pressure X-ray diffraction, ultrasonic measurements, Brillouin scattering technique, strain gauge method, etc., are needed to retrieve reliable data on the elastic modulus of superhard materials

3. HIGH ELASTIC MODULI AND PROBLEM OF "IDEAL" MECHANICAL CHARACTERISTICS

The existence of correlations between hardness and unambiguously determined physical characteristics is extremely important for the search for new superhard materials. The interrelation between the hardness and the molar volume of a substance or its density as well as the correlation of the hardness and elastic characteristics of a substance, are of special interest. The elastic moduli of a substance, unlike its hardness, depend only on the interatomic interactions. Elastic moduli of a polycrystalline material depend basically on the interatomic interactions except very specific cases of textured materials. The first-principle calculations of elastic moduli of materials are quite a routine problem at present. It is obvious that high-hardness materials should be searched for among substances with high elastic moduli [50].

A good correlation is observed between the shear modulus and hardness. The hardness and Young modulus are correlated somewhat poorer, whereas there is no monotonic interrelation between the hardness and bulk modulus (Fig. 1). By its very definition, the hardness is related to the process of shear deformation under the indenter rather than isotropic compression. As it was shown, the ideal hardness, being the upper elastic limit of the actual hardness, is unambiguously controlled by the Young modulus value.

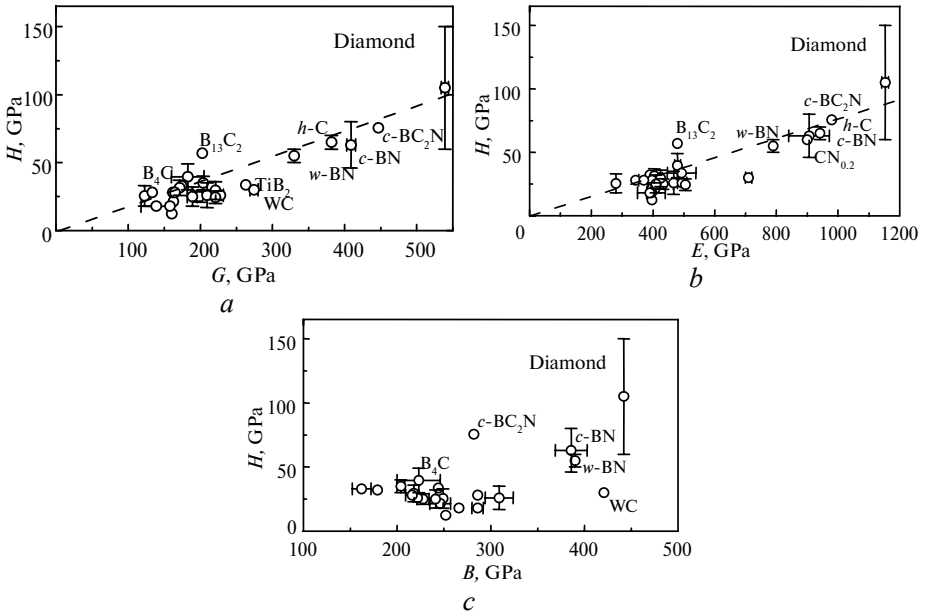

Fig. 1. Hardness vs. shear (*a*), Young's (*b*), and bulk (*c*) moduli dependences for superhard materials according to the data collected by Brazhkin et al. [5]. Dashed lines illustrate the correlations between hardness and shear or Young's moduli.

Summarizing, elastic moduli, primarily the bulk modulus, are controlled mainly by the atomic or, in a more general case, electron valence density, and the search for superhard materials should be conducted among substances with high values of the atomic and electron density and high bonding energies.

It seems extremely important for creating new superhard materials to understand the role of purely geometric characteristics of the structure, such as the number of nearest neighbors, angles between the bonds, etc. The idea, that the covalent structure must become more rigid with the increasing number of nearest neighbors (the coordination number) can be quite clearly explained theoretically in the framework of the concept of rigidity percolation [51]. At the critical coordination number $\langle z \rangle_c = 2.4$, the covalent network must become mechanically rigid. The model calculations for covalent networks in the general case or for amorphous sp^2–sp^3 carbon networks completely support this approach [52]. Therefore, from the standpoint of the search for superhard materials, only the structures with $\langle z \rangle \geq 3$ can be evidently of interest.

As was shown above, the natural limitations to elastic moduli consequently constrain ideal mechanical characteristics, including the ideal hardness. The elastic moduli and ideal hardness are completely controlled by the distribution of the electron density of valence electrons in metals and by geometry of the atomic structure. However, a wide gap between the real and ideal hardnesses or strengths (for superhard materials, the ideal and real parameters differ by a factor of 3 to 10) stimulates the search for means, which would be capable of bringing the hardness and other mechanical characteristics closer to their ideal values. The control of the system morphology is the key way to the solution of this problem (Fig. 2). We will not consider composite materials or superlattices, which display distinguished mechanical properties, and focus on the nanomaterials.

The hardness and strength of the material are known to increase and approach their ideal values in two limiting cases: (i) for a defectless single crystal containing

virtually no dislocations (for example, single-crystalline whiskers) and (ii) for the amorphous or nanocrystalline state. In the latter case, the formation and motion of dislocations is difficult due to a defective structure of the material at the nanometer scale.

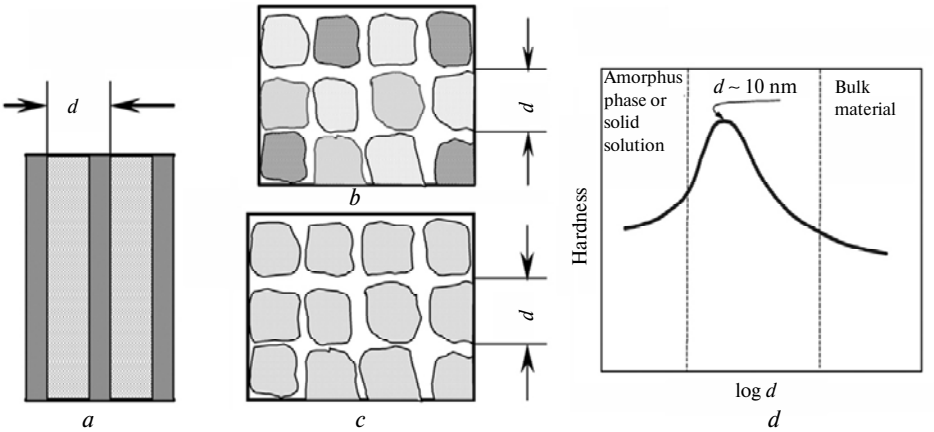

Fig. 2. Nanostructured materials, including superlattices (*a*), multicomponent (*b*), and single-component (*c*) nanocrystalline composites, may demonstrate the maximum of hardness (*d*) for a definite size of crystallites or superlattice period.

The nanostructures with the grain of sizes ~ 5–10 nm are optimal from the standpoint of the maximum hardness [53, 54] (see Fig. 2). The existence of the optimal grain size is quite explicable. With a decrease in the grain size d and the corresponding increase in the fraction of inter-granular boundaries, the value and density of barriers for the motion of dislocations increase. In this case, the known Hall-Petch law $H = H_0 + Ad^{1/2}$, where d is the grain size, is observed for the hardness. However, for very small grains, the number of atoms at intergranular boundaries and inside grains becomes comparable. In this case, intergranular boundaries cease to be barriers for the motion of dislocations, and the mechanism of the intergranular slip set to work. The size of the dislocation core becomes in this case comparable with the grain size, i.e. the dislocation does not feel any inhomogeneities on its path. A substantial progress in understanding the corresponding processes has been gained due to the works on computer simulation [55].

Nanopolycrystals actually possess unique mechanical properties. Thus, natural diamond polycrystals with ultrafine grains (carbonado) substantially exceed ordinary diamond single crystals in hardness and cracking resistance. Unfortunately, polycrystalline materials with fine grains are very difficult to obtain. Conventional methods of quenching from the melt yield the grain size of at least 100 nm. As a result, the standard approach to the obtaining of nanocrystals is the compaction (pressing) of nanoparticles. In this case, the resulting porosity, chemical admixtures, and stresses at intergranular boundaries prevent the obtaining of the material with the optimal mechanical properties. Thus, the composites prepared by the compaction of diamond nanoparticles usually have hardness of 20–40 GPa. However, there exists an alternative method for obtaining nanocrystals through the crystallization from the amorphous state. In particular, as we will show below the pressure heating of amorphous carbon with the large fraction of sp^3 states obtained from fullerite produces the nanocomposite consisting of diamond and graphite grains of size 3–5 nm. Such a material, despite a substantial fraction

of the graphite-like phase, has the hardness $H \approx 120$ GPa and fracture toughness $K_{Ic} \approx 20$ MN/m$^{3/2}$, which is higher than the corresponding values for a diamond single crystal [28]. Very recently, diamond nanopolycrystals were obtained through the direct fullerite–diamond and graphite–diamond transition under pressures above 20 GPa [41], as well as from nanotubes, also by heating under pressures exceeding 20 GPa [56]. Diamond polycrystals consisting of nanograins have extremely high hardness (above 140 GPa at a load of 10 N).

4. EXPERIMENTAL

In a further discussion, we mainly deal with carbon materials obtained by thermobaric treatment of a fullerite C_{60} followed by quenching to normal conditions. "Toroid" chambers of various sizes were used for creating a high pressure with a maximum up to 17 GPa. For moderate pressure generation (below 2 GPa) we used a large piston–cylinder apparatus and gasostatic high-pressure apparatus. The synthesis of fullerite-based samples was carried out from a powder containing no less than 99.9 % of C_{60} with crystal grains of size ~ 0.1 mm. The structure of the samples was studied by X-ray diffraction (CuK_α and CrK_α). The structure of the samples was also examined using a JEM 2010HR (JEOL) transmission electron microscope operating at 200 kV. The microstructure of the samples was characterized by bright-field (BF) and high-resolution transmission electron microscopy (HRTEM), as well as by selected area electron diffraction (SAED). The density of the samples ρ was measured by the Archimedes method. The electron energy loss spectra (EELS) of the B-*K*, and C-*K* edges were detected with a GIF2000 (GATAN) parallel electron energy-loss spectrometer. The Raman scattering measurements were performed at 300 K using a Dilor XY system with a 514.5 nm Ar^+ ion laser as an excitation light.

The hardness of the samples was measured independently by means of three different techniques. The Vickers hardness H_V was found by a PMT-3M instrument at 5 N loading. To obtain the correct data of the sizes of imprint, a thin layer of paint was applied to a polished surface of the sample. Hardness measurements of the sample have also been performed with a microhardness tester (Duramin-20, Struers) under 1 to 10 N loads (H_1 notation). In-situ measurements of the hardness (H^* notation) were carried out using Nano Indenter – II (MTS Systems Inc., Oak Ridge, TN, USA). It was also used for measuring the Young modulus (E). The Vickers hardness H_V and the fracture toughness (crack resistance) factor were calculated according to the procedure proposed in [57]. The elastic moduli (the bulk (B), shear (G), and Young (E)) were independently found through ultrasonic measurements of the transverse and longitudinal velocities in the 5–10 MHz frequency range.

More experimental details can be found in the original papers [18, 21, 22, 24, 26–28, 40].

5. DIAGRAM OF TRANSFORMATIONS OF FULLERITE C_{60}

A wide variety of ordered or disordered carbon phases synthesized from fullerite C_{60} by the application of high pressures and temperatures has been discussed in many papers (e.g., in [4, 5, 7, 8, 43, 44]). Under high pressure C_{60} molecules become close to each other and different kinds of polymerization between the molecules occurs (Fig. 3). On the other hand at high temperatures the destruction of the molecules and transition to the atomic carbon phases takes place. Typical X-ray diffraction patterns for several key phases are shown in Fig. 4. Whereas polymerized phases may be considered as molecular modifications of C_{60},

many of which can be depolymerized back to the starting fullerite (see, for example, [6, 58] for 2D and [24] for 3D polymers), disordered and nanocrystalline sp^2–sp^3 phases have an atomic-based structure, corresponding to irreversible destruction of the C_{60} molecules.

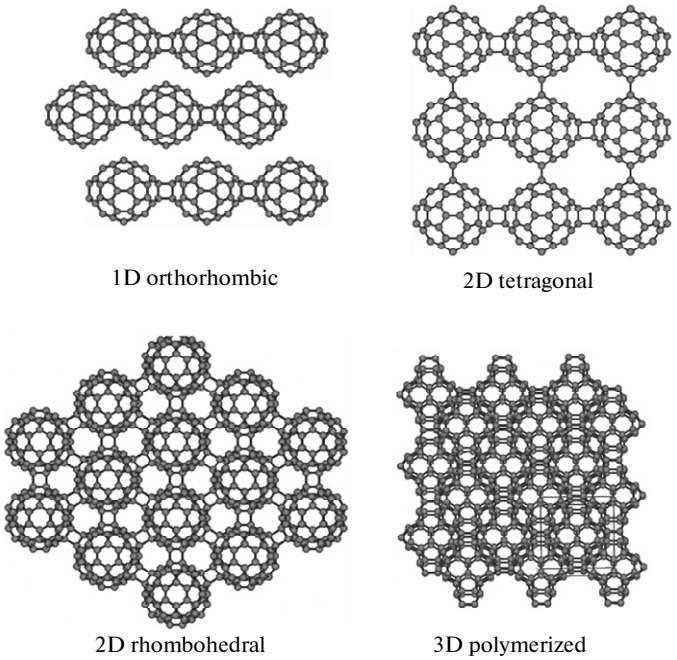

Fig. 3. Illustration of 1D, 2D, and 3D polymerized phases percolation of fullerite C_{60}.

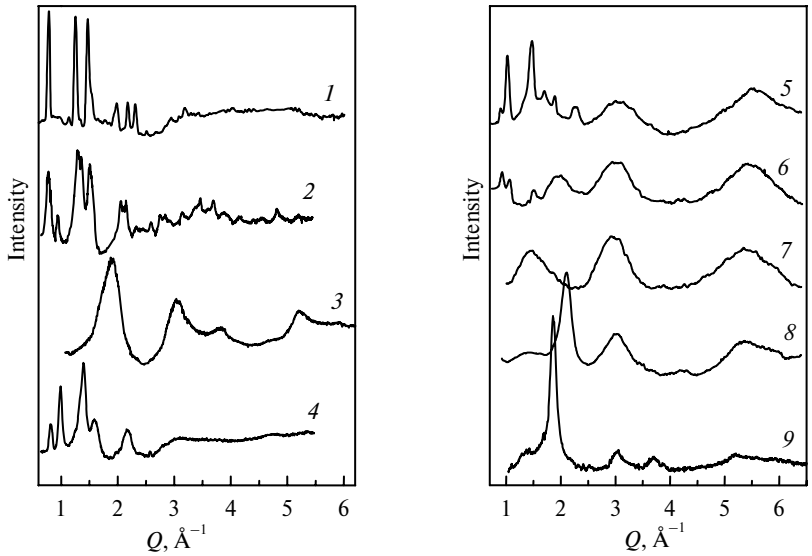

Fig. 4. Typical X-ray diffraction patterns taken at ambient conditions for carbon phases prepared from C_{60}. The corresponding structures were identified as follows (in parentheses the synthesis pressure and temperature are shown): (*1*) pristine C_{60}; (*2*) 2D polymerized rhombohedral phase of C_{60} (5 GPa, 970 K); (*3*) disordered atomic-based sp^2 phase (8 GPa, 1470 K); (*4*) and (*5*) 3D polymerized fullerite C_{60} with different lattice parameters (12.5 GPa, 470 and 570 K); (*6*) – strongly disordered 3D polymerized phase (12.5 GPa, 720 K); (*7*) and (*8*) disordered (amorphous) sp^2–sp^3 phases with different nanomorphologies and sp^2/sp^3 ratios (12.5 GPa, 770 and 1170 K); (*9*) diamond–graphite nanocomposite (12.5 GPa, 1670 K).

A kinetic transitional phase diagram of structural transformations of C_{60} fullerite is presented in Fig. 5. This diagram is constructed with regard to both original results and published data. The phase-transition curves in the monomeric C_{60} phase and the regions of the formation of 1D and 2D poly-fullerenes are reproduced from [12] and [43, 44], respectively. The stability boundary of these phases (up to 8 GPa) is taken from [12] with taking into account the phase diagrams from [8, 44] and the data from [9, 18]. A concentration isoline for dimerization of C_{60}, i.e. the line of fixed fraction of $(C_{60})_2$ dimers in the fullerite, is first constructed in this diagram with regard to the results obtained in [59, 60]. The region $p > 10$ GPa is presented according to the results of our works [24, 26] and data from [30–32]. This version of phase diagram has been presented for the first time in [61].

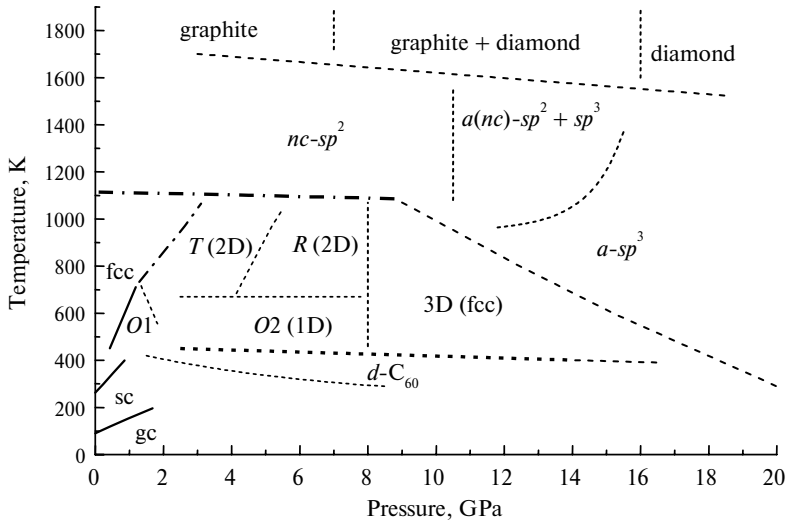

Fig. 5. Nonequilibrium (kinetic) transitional pressure-temperature phase diagram of C_{60}. Solid lines correspond to the thermodynamic phase boundaries for monomeric C_{60} phases; dot-and-dash lines correspond to the irreversible but sharp structural transformations; dashed lines correspond to the rather smooth transformations and separate regions of different classes of structures synthesized from C_{60}. The corresponding phases or classes of structures are designated as follows: fcc, sc, and gc correspond to the fcc, primitive cubic, and orientational glassy phases (all monomeric); *O*1, *O*2, *R*, and *T* are low-pressure and high-pressure 1D orthorhombic phases, and 2D rhombohedral and tetrahedral phases; *d*-C_{60} are phases with a predominant concentration of $(C_{60})_2$ dimers; *nc*–sp^2 are disordered (nanocrystalline) graphite-like phases; 3D (fcc) are 3D polymerized C_{60} phases; *a*–sp^3 and *a*(*nc*)–$sp^2 + sp^3$ are amorphous phases with possible nanocrystalline inclusions in the second case.

The high-temperature region at pressures below 1.5–2 GPa has not been considered previously in details. Recently we have found that this part of the transitional phase diagram has its own peculiarities. At $p < 2$ GPa, the temperature stability of fullerite C_{60} to molecular destruction at heating is by 100–150 K higher than that at high pressures $p > 3$ GPa. Moreover, the structure of disordered carbon phases, obtained at heating the C_{60} fullerite at moderate pressures, differs considerably from that of nanographite modifications obtained at high pressures $p >$ 3 GPa (see below). The possibility of the production of hard carbon materials from C_{60} fullerites at $p < 2$ GPa has not been looked into thus far, although it is known that the heating of C_{60} at ambient pressure leads to the formation of amorphous carbon at $T > 1200$ K. It should be noted that the breakup of the molecular structure

and the formation of hard nanographite phases at $p > 2$ GPa takes place through intermediate polymerized C_{60}-based modifications, since at $p < 2$ GPa the destruction of molecules at heating should occur directly in the initial molecular phase C_{60} [43, 61]. We will consider the transformation of fullerite to hard carbon phases in this moderate-pressure region in more details in Section 7.

We emphasize that this diagram does not have conventional characteristics and, basically, cannot be unambiguous. The structure of the formed phases may depend, not only on the kinetic conditions of the experiment (see, for example, [9, 59]), the path in the p, T plane, and the hydrostatic conditions, but also on the starting orientational state of C_{60} molecules [62]. We distinguished between three classes of lines (see Fig. 5): phase boundaries for the monomeric C_{60} phase, which were determined thermodynamically for the molecular substance; lines of sharp structural transformations, such as the stability boundary of polymolecular phases; regions of gradual transformations, such as dimerization and 1D, 2D, or 3D polymerization, where the line has a fully conventional character and can be constructed in a physically definite way only from the percolation point of view.

The diagram of transformations presented here for the region of high pressures > 10 GPa is notably different from that proposed previously in [25, 63], which was repeatedly reproduced in a number of reviews, for example, in [43, 44]. The point of view presented in this work is confirmed by synchrotron studies [14, 30, 32].

The pressure area in the presented diagram is restricted to 20 GPa and approximately corresponds to the stability pressure interval of C_{60} for compression at room temperature. Although there were intensive studies of C_{60} compressed to this and higher pressures at room temperature [64–73], the picture of transformations of C_{60} at compressions above 20 GPa is still not completely clear. The presented transitional diagram also does not reflect the data of shock–wave experiments [38, 39, 74], where an amorphous diamond has been obtained, since the corresponding experimental points are beyond the boundaries of this diagram. The points corresponding to the recent results on preparation of superhard nanocrystalline diamond [41, 42] lie near the top right corner of our diagram.

6. ZONES OF HARD CARBON PHASES

Since C_{60} molecules interact via only weak Van der Waals forces, pristine C_{60} is a very soft material with hardness $H \approx 0.4$ GPa [18]. Polymerization is a natural way for hardening this material, because covalent bonds between molecules are much stronger than molecular forces. But 1D and 2D C_{60} polymers are still rather soft materials with hardness $H \approx 1$–2 GPa [18, 20].

Only application of high pressure and/or high temperature provides the way to synthesize hard and superhard carbon materials. In this respect, one can select the three regions of hard phases at the transitional phase diagram (see Fig. 5): (i) the region of disordered sp^2-type atomic structures obtained at moderate pressures up to 8–10 GPa and high temperatures >1100 K, (ii) the region of three-dimensionally polymerized C_{60} phases synthesized at moderate temperatures of 400–800 K and high pressures > 8–10 GPa, and (iii) the region of diamond-based amorphous and nanocomposite phases obtained at high pressures > 10 GPa and temperatures > 800 K. Below, we consider the particular properties of carbon phases synthesized in these three regions.

One of the most striking phenomena was first observed by Kozlov et al. [17], when the hardness increased by more than one order of magnitude due to the destruction of the C_{60} molecular structure by heating to ~ 1000 K at a relatively low pressure about 3 GPa. The similar picture of transformation to disordered

atomic-based graphite-type phases during heating is observed up to 8 GPa [18]. The above-mentioned pressure and temperature parameters restrict approximately the boundaries of the first region of hard materials prepared from C_{60}. No density jump was observed within the acceptable range of experimental accuracy, whereas a substantial structural reconstruction from a molecular polymer to a disordered sp^2 network (Fig. 6) occurred [18]. The hardness of disordered phases seems to be independent of pressure, though the density somewhat increases in the pressure interval from 3.5 to 8 GPa. The variation of elastic moduli is not so drastic: the B and G moduli increase by a factor of 4 to 5 and 2 to 3 times, respectively, while the hardness of disordered structures is 100 to 200-fold greater than that of graphite (see Fig. 6). The reasons for superhard properties of disordered atomic-based graphite-type phases obtained from C_{60}, in spite of graphite being a soft material, will be discussed in the next sections. The moderate pressure-high temperature region of disordered sp^2 network formation (below 2 GPa) has been studied only recently. The carbon phases prepared in this region has some specific features and they will be considered separately in Section 7.

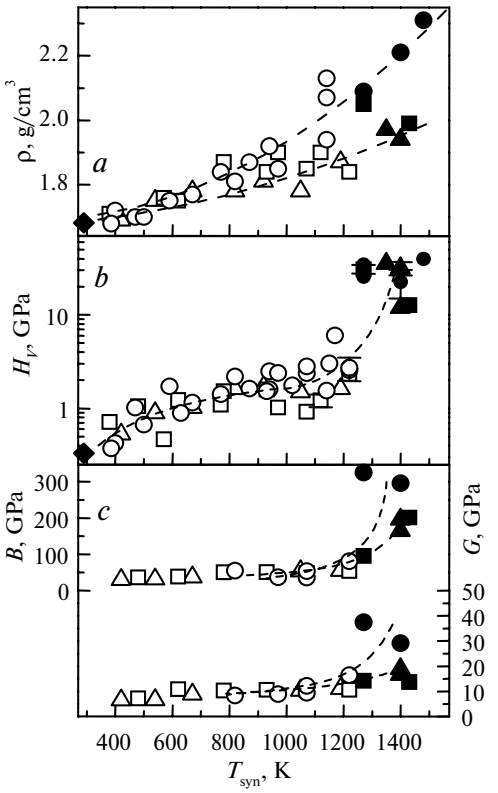

Fig. 6. Dependences of (*a*) density, (*b*) Vickers hardness, and (*c*) ultrasonic elastic moduli for samples synthesized from C_{60} pristine (◆) at pressures 3.5 (△, ▲), 5 (□, ■), and 8 (○, ●) GPa. Open symbols correspond to 1D and 2D C_{60} polymerized phases, and solid symbols correspond to disordered graphite-like phases. Dashed lines are the guides for eyes.

Among polymeric modifications of C_{60}, only 3D polymerized C_{60} phases correspond to hard carbon materials. The area of high pressure between 9 and 20 GPa and moderate temperatures in the range of 500 to 1000 K is the second pressure–temperature region, where one can synthesize hard 3D polymers of C_{60}. The appearance of strong covalent bonds between C_{60} molecules in all three dimensions is the key property of 3D polymers resulting in their superhard mechanical characteristics.

3D polymerization is a gradual process occurring with the increase of temperature (see Fig. 4) [13, 14, 24, 26–37]. The structure of all crystalline polymerized phases prepared can be identified as fcc with the lattice parameter a decreasing with the synthesis temperature increase. The identification of polymerized phases as the fcc structures with various lattice parameters [13, 14, 22–30] is rather typical for C_{60} even at low pressures [6, 18, 75]. At the same time, there is evidence of existing 3D polymers with the molecular arrangement distorted with respect to the fcc structure [22, 25, 33–37, 76]. Moreover, the observation of the Debye-Scherrer ellipses from 3D C_{60} polymers [77] demonstrates a systematic distortion of the cubic molecular short range order structure as the memory

signature of anisotropic pressure. Here, one should emphasize that all the experimental X-ray diffraction patterns of 3D polymers display at most 5 to 6 crystalline reflections, which is clearly insufficient for a precise identification of such complicated structures as C_{60} polymers.

Recently, a number of hypothetical 3D polymerized C_{60}-based ordered structures have been proposed [78–86]. These structures are of interest for recognizing possible covalent configurations of the nearest neighbor molecules in 3D polymerized phases, but the available experimental data on 3D polymers cannot be described in terms of the strictly ordered crystalline molecular structure. The experimental 3D polymerized C_{60} phases seem to be orientationally disordered. The reasons for this are connected with the orientational randomization in pristine C_{60} and non-synchronous character of the formation of covalent bonds between different nearest neighbor molecule pairs. Only the application of pressure to 1D and 2D C_{60} polymers can probably provide the experimental way for synthesis of the ordered 3D polymers similar to those proposed theoretically [78–86], and there has been an initial experimental attempt [15, 16, 33–37, 87] in this respect.

In the subsequent discussion, the 3D polymers will be considered as effective fcc molecular structures with the intention of correlating the molecular center positions. The two stages of 3D polymerization can be distinguished [26] from experimental X-ray diffraction data: (i) a gradual formation of covalent bonds between molecules, probably, via the [2 + 2] cycloaddition mechanism [88] (for the lattice parameters of fcc structures $a \geq 12.3$ Å); (ii) the appearance of additional covalent bonds ("overpolymerization") between molecules and simultaneous distortion of the initially spherical C_{60} units interconnected within the polymerized structure skeleton ($a < 12.3$ Å) and activation of the [3 + 3] cycloaddition mechanism of polymerization [87].

For describing the transition from the soft pristine C_{60} to strongly polymerized superhard 3D structures, it is adequate to use the elastic rigidity percolation theory [51, 89], which should operate with the degree of covalent bonding between molecules, if we consider the contribution of van der Waals forces to be negligible. A 3D network of covalently bonded atoms becomes rigid, when the average coordination number exceeds the value of $Z_c = 2.4$ [89]. The average coordination number for covalently bonded pairs of C_{60} molecules Z_p would be defined by their share n_p as $Z_p = n_p Z$, where $Z = 12$ is the coordination number of a fcc lattice. Considering the threshold covalent intermolecular coordination number for the appearance of hardness and elasticity in a system of partially covalently bonded C_{60} molecules to be equal to $Z_c = 2.4$, similarly to a covalent atomic network, we obtain the threshold concentration $n_c = 0.2$ and the corresponding lattice period $a_c \approx 13.8$ Å (in the framework of the model proposed in [24, 26, 27]). Figure 7 shows the dependence of the hardness for the 3D polymerized fcc phases of fullerite C_{60} on the lattice parameter, which completely supports the picture following from the percolation theory. The hardness continuously increases with the average coordination number for molecules, similar to the increase of elastic constant in the model of rigidity percolation [89]. Linear interpolation with the least squares fitting gives the threshold parameter close to the estimated value $a_c \approx 13.7$ Å.

The heating of C_{60} to temperatures higher than the range of the 3D polymerization at pressure higher than ~ 12 GPa (particularly, to 800 K or to higher temperatures at 12.5 GPa [26]) leads to a destruction of the molecular structure and formation of disordered atomic-based phases. The typical phases obtained during heating at 12.5 GPa are illustrated by the X-ray diffraction data in

Fig. 4. Nominally, we consider the third region of superhard materials (see Fig. 5). The temperature of disordering (amorphization) is pressure-dependent [65]. The details of the structural analysis of the diffraction patterns and Raman spectra for the disordered phases are described elsewhere [26, 28, 40]. One can select the following types of high-pressure disordered materials: (i) diamond-like (basically sp^3) amorphous phases; (ii) sp^2–sp^3 nanocomposite amorphous phases consisting of both diamond-type and graphite-type clusters; (iii) diamond–graphite nanocrystalline composites. From the width of diffraction peaks, one can estimate the sizes of structurally coherent clusters at ~ 10–20 Å for amorphous phases and at ~ 30–50 Å for nanocrystalline composites. There is some evidence of existing angular correlations in cluster orientations in the disordered phases [90], similar to those observed for disordered graphite-type phases obtained at lower pressures [76]. With increasing pressure, the fraction of graphitic-type (sp^2) clusters vanishes and fullerite C_{60} undergoes temperature-induced transformation to amorphous [38, 39] and nanocrystalline [41, 42] diamond.

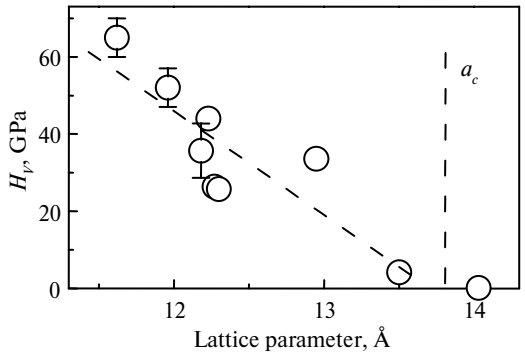

Fig. 7. Vickers hardness of the 3D polymerized C_{60} phases as a function of the lattice parameter. Dashed lines are the guides for eyes. The vertical dashed line corresponds to the rigidity percolation threshold a_c. The hardness of the least-dense sample (a = 14.4 Å) is equal to 0.15±0.05 GPa.

7. HARD CARBON MODIFICATIONS PREPARED FROM FULLERITES AT MODERATE PRESSURES AND HIGH TEMPERATURES

The large set of samples was produced in a piston–cylinder high-pressure device at synthesis pressures p_{syn} from 0.5 to 1.5 GPa and temperatures T_{syn} from 1100 to 1600 K. Besides, several samples were obtained at $p_{syn} \approx 0.15$–0.2 GPa in a gas cell with the use of nitrogen gas pressure. The duration of the temperature treatment under pressure was ~ 5–10 min. The samples of carbon phases synthesized at pressures 0.15–1.5 GPa have quite low density between 1.6 and 1.9 g/cm^3, while for the synthesis pressures 3–15 GPa the density is 2–2.8 g/cm^3 (table).

The selected typical structural data for the nanocarbon phases are presented in Fig. 8. The structure of the samples obtained at moderate pressures is noticeably different from that of nanographite phases prepared at high pressures $p_{syn} > 3$ GPa. The main maximum of the structure factor of carbon phases obtained at low pressures corresponds to the wave vector value $Q \approx 1.3$ Å^{-1}, which is far from the main graphite peak (at ~ 1.87 Å^{-1}) and fairly close to the (220) line of molecular C_{60} (at ~ 1.25 Å^{-1}), determined by the distances between the centers of the C_{60} molecules, $d = 4\pi/Q_{(220)} \approx 10$ Å. At the treatment temperature exceeding 1300 K, an additional maximum, along with the first one, appears at $Q \approx 1.8$ Å^{-1}, which can be clearly associated with expanded graphite. The intensity of the maximum at $Q \approx 1.8$ Å^{-1} increases with the rise of the treatment temperature, while the peak

intensity at $Q \approx 1.3$ Å^{-1} decreases. If the treatment pressure exceeds 3 GPa, the main peak of the structural factor corresponds to nanocrystalline graphite ($Q \approx 1.85$–1.9 Å^{-1}), and the halo at $Q \approx 1.3$ Å^{-1} is observed only in a narrow range of the synthesis temperatures from 1100 to 1250 K.

Synthesis conditions (p_{syn} and T_{syn}), density (ρ), elastic moduli (B, G, and E) from ultrasonic measurements, Young modulus from the nanoindentation curves (E^*), hardness (H) measured by different techniques, H/E ratio (where the hardness and Young modulus are averaged from different techniques), and elastic recovery (R) for different nanostructured carbon phases. Details of the notations are presented in Section 4. The last row shows absolute uncertainties

N	p_{syn}, GPa	T_{syn}, K	ρ, g/cm^3	B, GPa	G, GPa	E, GPa	E^*, GPa	H, GPa	H_1, GPa	H^*, GPa	H/E	R, %
1	0.15	1300	1.6	15	12	28	28	4	3.7	3.5	0.13	78
2	0.5	1200	1.75	16	13	32		5	5.2		0.19	89
3	0.5	1350	1.75	26	18	44	45	6.5	7	7.5	0.16	83
4	0.75	1380	1.8	31	20	49		8.5	8		0.17	
5	0.75	1420	1.75	31	20	49		8.5	7.5		0.17	
6	1.1	1200	1.81	28	18	44.5		8.5	7		0.17	
7	1.1	1250	1.82	33	21	52	56	8.5	6.5	9	0.17	89
8	1.1	1300	1.82	35	22	55	57	8.5	7.5	10.2	0.18	88
9	1.2	1400	1.78	35	22	55	59	11.5	12.5	12.8	0.22	92
10	1.4	1500	1.87	42	17	46		6	5.5		0.14	
11	3.5	1200	1.95				59	8		9	0.13	77
12	3.5	1400	2.05				77	10.5		11	0.13	79
13	7.0	1150	2.2				115	18		16	0.14	82
14	7.0	1350	2.25				80	11		11.5	0.14	82
15	12.0	1100	2.5				98	13		12	0.13	80
16	15.0	800	2.8				410	55		46	0.12	93
17	15.0	1100	2.8				130			17	0.13	90
±Δ	0.05–0.2	30–60	0.05	2	2	3	2	1.5	1	0.5	0.03	3

The TEM patterns from the samples (Fig. 9) confirm the X-ray diffraction evidence that the structure of the nanocarbon modifications prepared at moderate pressures and temperatures $T_{syn} \approx 1300$ K incorporates interlinked curved molecular fragments, while at $T_{syn} \approx 1500$ K the material is mainly composed of graphite nanograins, although the atomic planes still show some curvature.

The Raman spectra (Fig. 10) are similar to those for disordered graphites and amorphous sp^2-based carbon modifications. Aside from the weak maxima near 450 and 800 cm^{-1}, all the spectra show two main maxima with the peak positions at 1330–1350 and 1580–1605 cm^{-1}. The given maxima are usually interpreted as corresponding to the D- and G-bands of disordered graphite [14, 17]. Note that the D-band, as a rule, is located at 1350–1360 cm^{-1}, and the G-band at 1580–1590 cm^{-1}, that is, the positions of the D- and G-bands in our experiments are slightly shifted. The lower is the synthesis pressure, the higher are the frequencies of the corresponding peaks in spite of the lower density of the samples. All features of the Raman spectra correspond to disordered carbon materials [91].

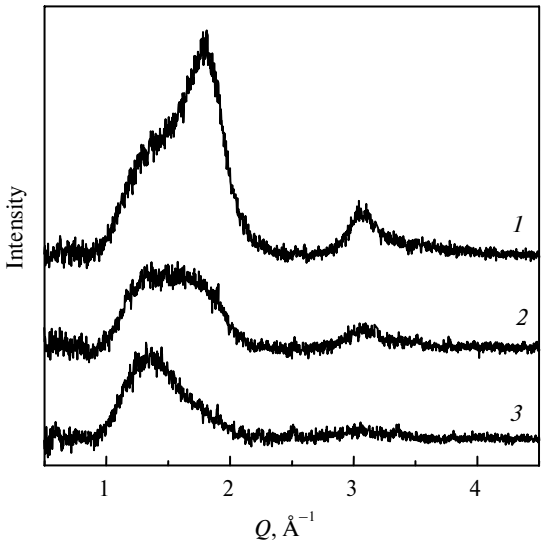

Fig. 8. X-ray diffraction patterns taken at ambient conditions from samples synthesized at low pressures. Pressure and temperature of synthesis mark corresponding patterns: (*1*) 1.4 GPa, 1500 K; (*2*) 0.5 GPa, 1350 K; (*3*) 0.15 GPa, 1300 K.

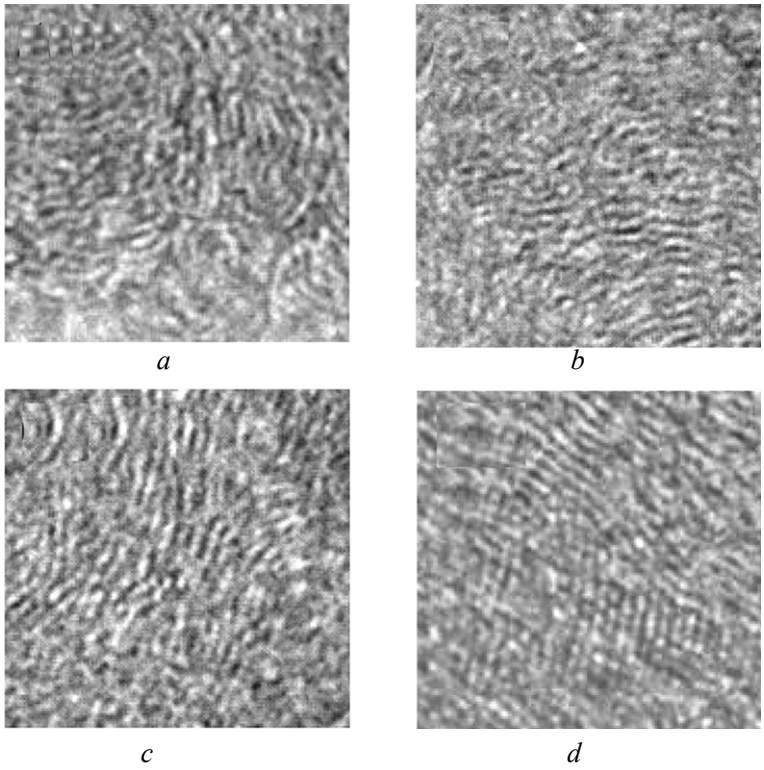

Fig. 9. Typical HRTEM images for high-temperature amorphous and nanographite phase synthesized from C_{60}. The synthesis conditions are the following: (*a*) 0.15 GPa and 1300 K, (*b*) 0.5 GPa and 1350 K, (*c*) 1.4 GPa and 1500 K, and (*d*) 8 GPa and 1300 K. Panel (*a*)–(*c*) correspond to X-ray diffraction data in Fig. 8. The size of images approximately corresponds to 10 nm.

The results for the hardness and elastic moduli for several typical samples are presented in table. The samples obtained at moderate pressures have sufficiently

high hardness values $H \approx 5$–15 GPa and the record high H/E ratio values ~ 0.18–0.22, as well as the record high values of the elastic recovery ~ 85–92 % (Fig. 11). It should be mentioned that for the nanographite modifications prepared at high pressure (3–15 GPa), the H/E ratio is around 0.1 with the maximum value ~ 0.14 (see table). The data on hardness and elastic moduli, obtained through various techniques, are in good agreement (see table). Let us note that the nanocarbon samples with hardness $H > 8$ GPa can easily scratch a tungsten carbide hard alloy with hardness $H \approx 15$ GPa, the capability attributable to the high elastic recovery of the new phases. The values of the elastic moduli for the hard carbon phases produced at moderate pressures exceed those for graphite despite the lower density, although being below those for carbon modifications obtained at high pressures $p_{syn} > 3$ GPa.

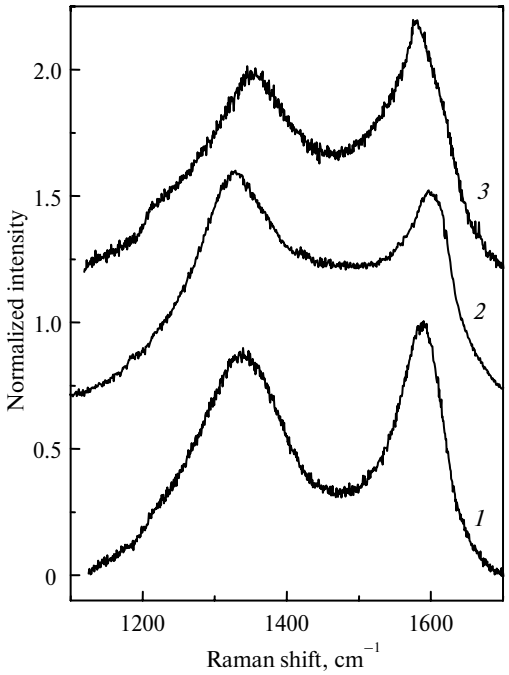

Fig. 10. Typical Raman spectra for nanostructured carbon modifications synthesized from C_{60} at high temperatures and at low, moderate, and high pressure: (*1*) 0.15 GPa, 1100 K; (*2*) 1.2 GPa, 1300 K; (*3*) 12GPa, 1300 K.

Thus, synthesis of nanocarbon modifications at moderate pressures in a narrow temperature region around 1400 K permits one to prepare a carbon material with high hardness and elastic recovery.

High hardness and the record elastic recovery values of the samples under study are evidently related to the peculiarities of their structure at the nanometer scale. In this structure, being in some respect similar to the structure of schwarzite-1248 and amorphous schwarzite [92, 93], the interlinked curved parts of the C_{60} molecules and graphite nuclei that grow and absorb the curved parts at heating are combined. It is interesting that the predicted Young modulus of amorphous schwarzite of ~ 29 GPa [93] is quite close to the value of the Young modulus of sample 1, namely 28 GPa. The randomness of the structure and the lack of "soft" directions ensure quite high values of the elastic moduli (by 1.5–2 times higher than those for graphite) in spite of the lower density. The difficulty of an intergrain sliding in the

given structure, heterogeneous at the nanoscales, causes hardness to rise, approaching its "ideal" level. The high elastic recovery can be explained in the framework of a "squeezed chicken wire" model [94]. In a C_{60} molecule, the bonds between carbon atoms, as distinct from graphite, are disparate as there are both single and double ones. After the breakup of a molecular structure, a considerable portion of the double bands is obviously retained in nanocarbon phases, and it leads to a slight increase in the Raman *G*-band frequencies.

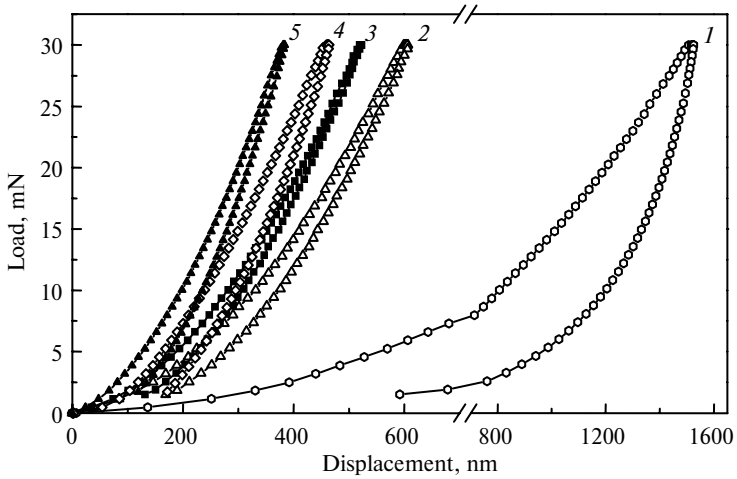

Fig. 11. Nanoindentation curves for nanostructured carbon modifications synthesized from C_{60} compared with that for ordinary high-quality dense graphite MPG 7 (*1*), pressure and temperature of synthesis: 0.5 GPa, 1350 K (*2*); 1.2 GPa, 1300 K (*3*); 3.5 GPa, 1400 K (*4*); 7.0 GPa, 1200 K (*5*).

At $p_{syn} > 2$ GPa graphitization of a polymer C_{60} phase at heating is an easier process than the graphitization of a molecular C_{60} in the pressure range of 0.15–1.5 GPa. This is due to the fact that the density of polymer C_{60} phases at $p_{syn} \approx 2$–10 GPa and $T_{syn} \approx 1000$ K is close to that for graphite, which facilitates an easy formation and growth of the nucleation centers. Part of carbon atoms (~ 10–20 %) in polymer phases is in the sp^3 four-coordinated states; after the destruction of molecules these atoms can serve as stress relaxation centers at the boundaries of the formed graphite nuclei. At moderate pressures of 0.15–1.5 GPa, a molecular C_{60} has a considerably lower density than graphite, and after the destruction of molecules it transforms into a disordered carbon state consisted of curved molecular fragments. Graphite nucleation begins only after significant overheating as a diffusion driven nano-recrystallization. As a result, a wide pressure–temperature region appears, in which a new nanomaterial, representing a nanomixture of nanographite nuclei and curved molecular fragments, emerges. At the ratio of the nanographite atoms to molecular fragments being around 3:1 (synthesized at $T_{syn} \approx 1400$ K) one can achieve mechanical characteristics close to the "ideal" level.

Minimal pressures of the synthesis of hard nanocarbon phases $p_{syn} \approx 0.15$ GPa employed in this work are dictated by the necessity to compact a pristine C_{60} powder. If one has large C_{60} fullerite single crystals, it seems possible to produce hard carbon nanostructured phases by heating the samples at ambient pressure. Moderate values of pressure ~ 1 GPa required to obtain nanostructured carbon with hardness ~ 10–15 GPa and elastic recovery ~ 90 % enable the synthesis of samples

of an optional shape of dozens cm in size, which is promising for industrial applications of these new materials.

8. AMORPHOUS DIAMOND-LIKE CARBON

Strongly disordered diamond-based carbon materials, prepared from C_{60} at high pressures and high temperatures and corresponding to the 3rd region discussed in Section 6, are of special interest since these materials reveal the highest record mechanical characteristics. It is well known that many mechanical properties of polycrystals improve as the grain size decreases [50, 54, 95]. In this connection, it is of enormous interest to synthesize diamond-based nanocomposites. However, because of the residual porosity, chemical impurities, and residual stresses at grain boundaries, the standard methods of compacting diamond nanopowders do not yield composites with high mechanical characteristics. An alternative method for obtaining a nanocrystalline state is crystallization of the corresponding amorphous phase. A distinctive feature of amorphous carbon modifications is that the average coordination number in them can actually vary from 2 to 4. It is natural to assume that amorphous phases with a large fraction of fourfold coordinated sp^3 states are preferred for obtaining diamond nanocomposites. To date amorphous modifications of carbon with a large fraction of sp^3 states have been synthesized only in the form of thin films [96]. The transformations of fullerite C_{60}, which were discussed above, open up new possibilities for obtaining three-dimensional samples of amorphous and nanocrystalline diamond-like carbon.

The amorphous carbon obtained from C_{60} contains an appreciable fraction of atomic sp^3 states at pressures of 8–9 GPa, where a crossover is observed between temperature-induced 2D and 3D polymerizations [4, 5, 39]. However, the amorphous network becomes predominantly four-fold coordinated only at pressures of 12–13 GPa [4, 5]. As a result, an appreciable yield of diamond from C_{60} without intermediate graphitization is kinetically reliable only at $p > 12$ GPa.

The amorphous samples obtained at lower temperatures of ~ 800–900 K at 12–13 GPa are uniform materials on a micron scale, while the high-temperature ~ 1000–1500 K samples have a complicated macroscopic morphology. The change in the morphology of the samples is due to the rearrangement of the structure on a nanoscale, while the sample remains amorphous on large scales. A crystallization of the amorphous nanocomposite starts near 1700 K at 12.5 GPa. At this temperature, diamond crystallites of appreciable size are formed, since in addition to the (111) reflection peak, there are weak (220) and (311) reflections, as are graphite clusters, since the peaks of the graphitic phase shift toward the exact positions of the (002) and (004) reflections of graphite. The crystallite sizes estimated from the widths of the X-ray peaks are ~ 50 Å for graphite and ~ 25 Å for diamond.

The data for the hardness and fracture resistance of amorphous and nanocomposite samples are presented in Fig. 12 (which also show the points corresponding to 3D polymers). The large variance in the values obtained for the hardness makes it impossible to establish a systematic dependence on the load or type of phase. Nonetheless, the measurement accuracy is sufficient to conclude that an appreciable increase in hardness to values characteristic for diamond is observed for nanocomposite phases with density in the 3.0–3.4 g/cm^3 range. The fracture resistance of such phases can be 1.5–2 times greater than the values for diamond 7–10 MN/m$^{3/2}$. Recently we have studied several amorphous sp^3-rich samples by nanoindentation technique. The hardness of 40–50 GPa and huge elastic recovery (97 %) have been found (Fig. 13).

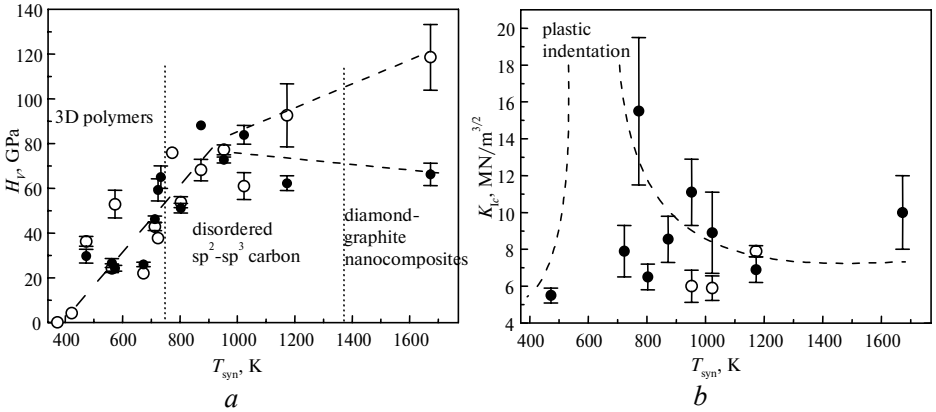

Fig. 12. Vickers hardness (*a*) and fracture toughness coefficient (*b*) vs. synthesis temperature for C_{60}-based carbon phases obtained at pressures of 12.5–13.5 GPa. The measurements were carried out at the indentation loads of 1.96 N (open symbols) and 5.42 N (solid symbols). The dashed lines are the guides for the eyes. In the interval of 600 to 700 K, the fracture toughness is not measurable.

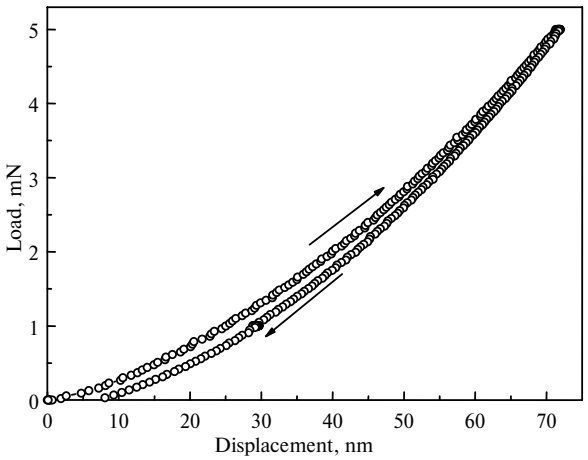

Fig. 13. Nanoindentation curve for nanostructured carbon modification synthesized from C_{60} at 16 GPa and 900 K. Analysis of this curve gives the following characteristics of the sample: hardness H = 41.5 GPa, Young's modulus E = 395 GPa, and elastic recovery R = 93 %.

One can make several remarks on the formation mechanisms of superhard sp^3 amorphous and diamond-based nanocomposite phases. Although the formal thermodynamic equilibrium of fullerite C_{60} with diamond lies at negative pressures, kinetic factors determine the real structural evolution of C_{60} under pressure. Specifically, at pressures up to 8 GPa, the fullerite–diamond transition occurs through graphitization, just as for amorphous carbon (soot) [97]. However, graphitization of soot is observed at least up to 15 GPa [97], whereas for C_{60}, the situation changes radically already at 12–13 GPa. An amorphous phase with a high fraction of sp^3 states (up to 80 %) forms in this pressure range at rather low temperatures of ~ 800 K. The convex shape of the spherical molecules makes it possible for them to approach one another effectively under pressure and lends a high capacity for the formation of covalent bonds between molecules, with the appearance of sp^3 states. At the same time, the extremely high stability of C_{60} molecules prevents the formation of graphitic clusters. The formation of a disordered network of atoms from 3D polymers apparently occurs without the

rupture of a large number of covalent bonds of the initial C_{60} molecules as structural units.

As the synthesis temperature increases, spatial separation of sp^2 and sp^3 atoms occurs (which is simply advantageous energetically), and first amorphous and then crystalline diamond-plus-graphite nanocomposites form. The yield of nanodiamonds accompanying crystallization of such an amorphous state reaches 50–80 %. The corresponding crystallization temperature (~ 1500–1700 K) is much lower than the temperature of the direct noncatalytic graphite-to-diamond transformation at these pressures.

It is interesting that the mechanical characteristics of the synthesized nanocomposites are extremely high, even though the materials contain a large fraction of graphitic clusters. Several reasons for such highest characteristics can be pointed out: (i) the optimal size of nanocrystallites (~ 50 Å) corresponding to the maximum hardness values; (ii) the uniform character of the formation of composites from rather soft molecular phases without nanopores, impurities, and distinct nanocrystallite boundaries; (iii) the formation of a rigid "skeleton" of diamond-like clusters; and (iv) the binding effect of graphite-like clusters, whose elastic recovery perpendicular to the graphene planes is anomalously high, whereas the strength of the planes against longitudinal stresses is very high.

Here we mainly discuss the disordered diamond (sp^3)-based phases obtained near 12–15 GPa, thus, containing a large fraction of sp^2 carbon (atomic sites or graphitic nanoclusters), but still being extremely hard materials with mechanical properties comparable to or exceeding those for diamond. With increasing the pressure and diminishing the fraction of graphitic-type (sp^2) clusters (atomic sites) to negligible or zero values, one can hope to obtain carbon materials, such as amorphous [38, 39] or nanocrystalline [41, 42] diamond, with higher mechanical characteristics.

9. CORRELATION BETWEEN DENSITY, STRUCTURE AND MECHANICAL PROPERTIES FOR NEW CARBON PHASES

A vast variety of carbon phases, pressure-synthesized from C_{60}, provide a unique possibility (e.g., comparing with other group IV elements) of experimental modeling of covalent structures with a variable bonding nature (in particular, the sp^2/sp^3 ratio), the effective dimension of covalent connectivity, the nanometer-scale atomic arrangement (cluster assembling), the degree of disorder, and so on. This offers a possibility of studying the correlation of various mechanical and physical properties of carbon phases with quite different structures. The correlations of this type are of general interest, because they give simple efficient criteria for predicting mechanical properties of novel and hypothetical carbon materials.

The correlations between the electron density (the ordinary density for particular cases) and elastic characteristics, as well as between the elasticity (first of all, the shear elasticity) and hardness exist in the general case of solids, including superhard materials [50, 98, 99]. In Fig. 14, we consider the Vickers hardness vs. density, $H_V(\rho)$, for different carbon phases, prepared from fullerite C_{60}, in comparison with the linear interpolation for the similar data on amorphous carbon films [96]. Both sets of the data are correlated fairly well. There is a clear tendency for an increase of hardness with density. The hardness increase for 3D polymerized C_{60} phases directly indicates the increase of the number of sp^3 sites in accordance with the well-known dependence of density on the share of sp^3 sites in amorphous carbon [96]. One should note that the materials discussed include both homogeneous (for the length scale of the medium-range order ~ 30 Å) and hetero-

geneous phases. The limited data (see e.g., [100–102]) on the hardness of materials synthesized from fullerites C_{70} or $C_{(2N)}$ (the mixture of various fullerene molecules, $50 < 2n < 180$) are consistent with the data presented in Fig. 14 for C_{60}-based phases.

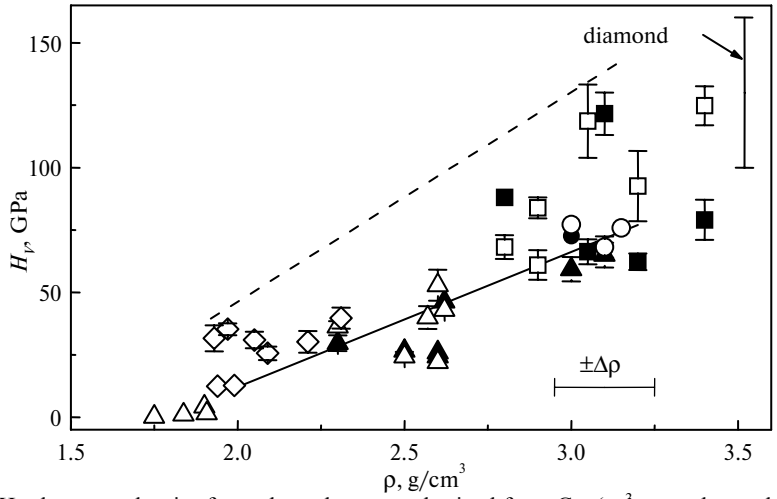

Fig. 14. Hardness vs. density for carbon phases synthesized from C_{60} (sp^3 amorphous phases are diamond-like). Open symbols correspond to an indentation load of ~ 2 N and solid symbols to ~ 5 N. The data on diamond are taken for loads of 2–5 N. Solid line corresponds to the dependence for amorphous films from [96] (——), 3D polymers (△, ▲), sp^2 nanographite (◇), sp^3 amorphous (○, ●), sp^2–sp^3 composites (□, ■). Dashed line is the boundary of maximum possible hardness values for carbon phases obtained from C_{60}.

Not only the atomic-level structure and interactions, but also the degree of homogeneity can vary in disordered and nanocrystalline forms of carbon and affect dimension mechanical properties. One can suggest that the dispersion of $H_V(\rho)$ points in Fig. 14 is related to the nanometer-scale morphology of samples. In particular, the disordered sp^2 phase and diamond-based nanocomposites correspond to the upper boundary of the $H_V(\rho)$ correlation area. Thus, the variation of the morphology, i.e. the structure and texture on a length of 10 to 1000 nm is another possibility for changing the properties of carbon materials.

One can suggest several reasons for the superhard property of disordered sp^2 phases, when their densities (see Fig. 6) are very close to that of graphite: (i) the nanometer-scale disorder of graphite-type covalent layers, providing the 3D arrangement of clusters with the 2D covalent geometry; (ii) a possible presence of sp^3 carbon sites adopted from the preceding 2D-polymerized phases; (iii) a high elastic recovery of the graphite-type structures orientationally disordered at the medium range order scale, similarly to fullerene-like (actually graphite) CN_x films [103]. Considering mechanical properties of the phase synthesized at low pressures, one should take into account a possible heterogeneity of samples, as well as anisotropy related to the 2D covalent topology of low-pressure phases [49, 104, 105]. From the point of view of the rigidity percolation theory (see previous section), the disordered sp^2 phases can be hard phases, since $Z = 3$ for them. But these phases should have a 3D atomic arrangement of covalent structure to be hard (covalently rigid) materials, opposite to soft graphite with an effectively 2D arranged covalent structure. The nanometer-scale cluster nature of the disordered sp^2 phases seems to cause the 3D arrangement of the atomic structure for $Z = 3$.

An even better correlation is observed between the bulk elastic modulus B and the density of carbon phases whose covalent structure is characterized by 3D ordering. In Fig. 15, experimental data for the disordered sp^2–sp^3 phases synthesized from C_{60} [18, 104, 106], for the 3D C_{60} polymers [33], and for the real allotropic carbon modifications are compared with numerous calculations for hypothetical phases, including amorphous structures [107], 3D C_{60} polymers [79, 80, 84], sp^2 crystalline phases [92, 108–111], and the high-pressure BC8 phase [112]. A good agreement basically between experimental and theoretical data is noteworthy. More detailed discussion on this subject can be found in [113]. One should note only that the phases with 1D or 2D covalent bonding (graphite and 1D or 2D C_{60} polymers), as well as the starting fullerite (a molecular van der Waals crystal with zero-dimensional covalent bonding), exhibit a much larger compressibility than the 3D bonded phases (see Fig. 15).

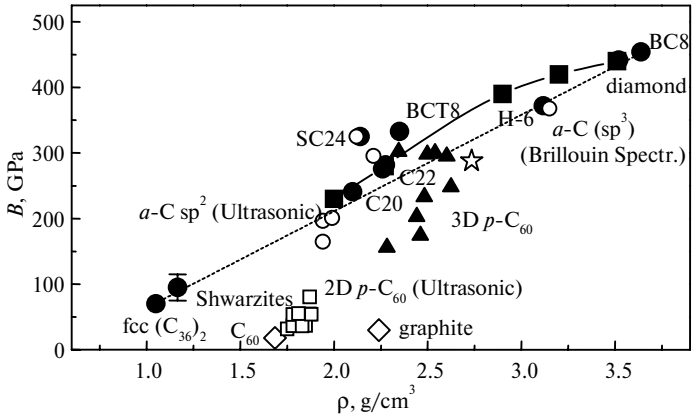

Fig. 15. Bulk modulus vs. density for allotropic carbon modifications and disordered phases (a-C) obtained from C_{60} (experimental methods are indicated in the figure) and calculation data for various hypothetical amorphous and crystalline phases: sp^2–sp^3 crystalline phases (●), 3D C_{60} polymers, calculation (▲), 3D C_{60} polymers, X-ray (☆), a-C (sp^2–sp^3) (■), a-C, experiment (○), 3D C_{60} polymers, experiment (□), Van der Waals phases (1D, 2D) (◇).

10. NONHYDROSTATIC STRESSES AND ANISOTROPY OF HARD CARBON PHASES

Fullerite C_{60} is a highly metastable phase with respect to ordinary graphite and diamond. Moreover, covalent carbon–carbon bonds are rather strong, causing large energy barriers for reconstruction of the carbon covalent structure. These circumstances result in specific features of the transitional pressure–temperature phase diagram of fullerite C_{60}. The first is the ambiguity of the carbon structure at a particular pressure–temperature point, since the structure of the obtained phase can strongly depend on the pressure–temperature path to the final point, as well as on the kinetic factors, such as the rate of a pressure or temperature change. The ambiguity of the product phase during a different scenario of the pressure–temperature treatment in the region of 1D and 2D polymerization (up to $p \approx 8$ GPa and $T \approx 1000$ K) is discussed in the original papers (e.g., [9–12]). One should also emphasize that transformation of fullerite C_{60} during room-temperature pressurization can depend on particular experimental conditions [64–73]. Previously we also mentioned the importance of the starting orientational state of C_{60} molecules in the pristine phase [62] and the possibility of different scenarios of 3D polymerization dependent on the mutual orientation of C_{60} molecules.

Particularly, there is an experimental evidence of the effect of a significant difference of the pressure–temperature and temperature–pressure paths on the product structure of the 3D polymer and its stability [35–37]. 3D polymerization processes of 2D polymers of C_{60}, preliminary obtained during some pressure–temperature paths, also differ from that observed for pristine C_{60} [87, 114].

Another important feature of non-equilibrium transformations in fullerite C_{60} under pressure, which we consider here in detail, is a strong influence of nonhydrostatic pressure conditions and shear stresses on the anisotropy of product phases. This effect is known now for 3D polymers of C_{60} [77, 106], hard disordered graphite-type (sp^2) phases [49, 104, 105], and 2D polymerized phases [49, 105, 115]. The pressure anisotropy naturally occurs in quasi-hydrostatic conditions that occur, for example, in a toroid-type apparatus with a single loading axis (z-axes in subsequent discussion).

In this respect, until now the bulk B and shear G moduli were calculated by using the isotropic medium approximation in the studies of the elastic properties of materials obtained from C_{60} [18, 116, 117]. Such calculations provided the values of Poisson's ratio that were anomalously high for covalent structures and the values of the bulk modulus that were nonphysically high [116, 117]. However, the possible orientational anisotropy and inhomogeneity of materials were not taken into account in these calculations.

A detailed study of elastic properties was carried out for the hard disordered graphite-type (sp^2) phases [49, 104] and the rhombohedral 2D polymerized phases [49, 105]. The values obtained for the density and the microhardness, ρ = 1.9–2.4 g/cm^3 and H_V = 21–32 GPa, are in good agreement with the data reported for disordered phases in earlier publications. A fundamentally new result of [104] is the strong anisotropy observed for the velocities of transverse and, especially, longitudinal ultrasonic waves propagating parallel and perpendicular to the z axis, which corresponds to the loading axis during the sample synthesis. The anisotropy of the velocities reaches 20–30 %. For microhardness, the values obtained with the indentation parallel to the z axis (H_z = 27 and 21 GPa for samples prepared at 1270 and 1450 K, respectively) and perpendicular to it (H_x = 32 and 27 GPa for the same samples) are also different, the microhardness anisotropy being within ~ 15–20 %.

The presence of anisotropy should be naturally attributed to the additional uniaxial pressure component that occurs in the quasi-hydrostatic conditions of the experiment. The X-ray diffraction data suggest that the sp^2 phases under consideration have a nanocluster structure, in which the clusters can have the form of graphite-like crystallites with a parallel atomic packing or an amorphous conglomerate of the partially ordered nanometer regions. The velocities of ultrasonic waves propagating along the graphite planes are known to be higher than the propagation velocities in the perpendicular directions. It is natural to attribute the anisotropy of the elastic properties observed in the experiment to the anisotropy of the spatial orientation of the structure-forming clusters, namely, to the presence of the preferred orientation of graphite-like planes that is normal to the z axis, which is the axis of additional uniaxial stress. The deviation from the spherically symmetric distribution of the orientation of graphite-like clusters leads to the formation of a sort of the texture in the disordered samples. The correlations between the elastic and ultrasonic anisotropy for both disordered graphite-type and rhombohedral 2D polymerized phases are illustrated in Figs. 16 and 17, respectively. More detailed analysis of these relations can be found in [49, 104, 105]. Transmission electron microscopy [118] and X-ray diffraction microtomography [119] highlighted that nanocluster structure, existing long-range correlations for orientation of clusters, lamellar and tweed

morphology and texture, and possible macroscopic anisotropy are intrinsic properties of the disordered graphite-type phases prepared from C_{60}, and all these properties can be recognized as a signature of stresses in the parent phase at different scales from the atomic level (atomic density modulation) to the macroscopic one (nonhydrostatic pressure environment).

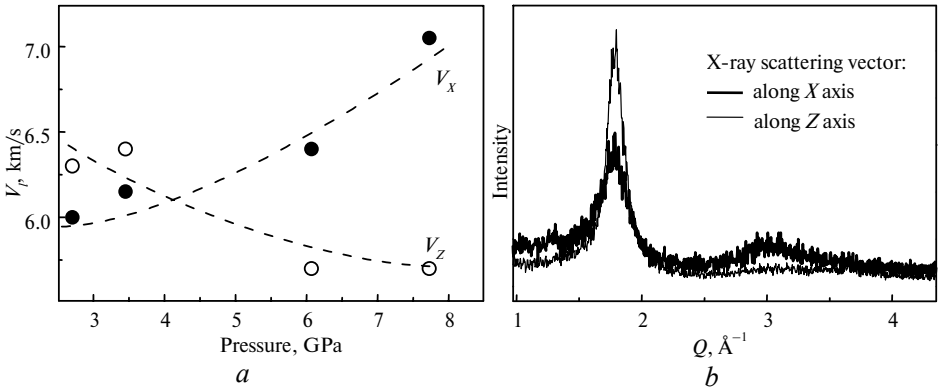

Fig. 16. Anisotropy of the nanographite phases revealed by longitudinal ultrasonic velocities plotted as a function of the synthesis pressure (*a*) and by X-ray diffraction patterns (with the subtracted middle lines) recorded in reflection mode for different geometries of the scattering vector (*b*). The *Z* axis corresponds to the pressure chambers load direction (additional uniaxial pressure component).

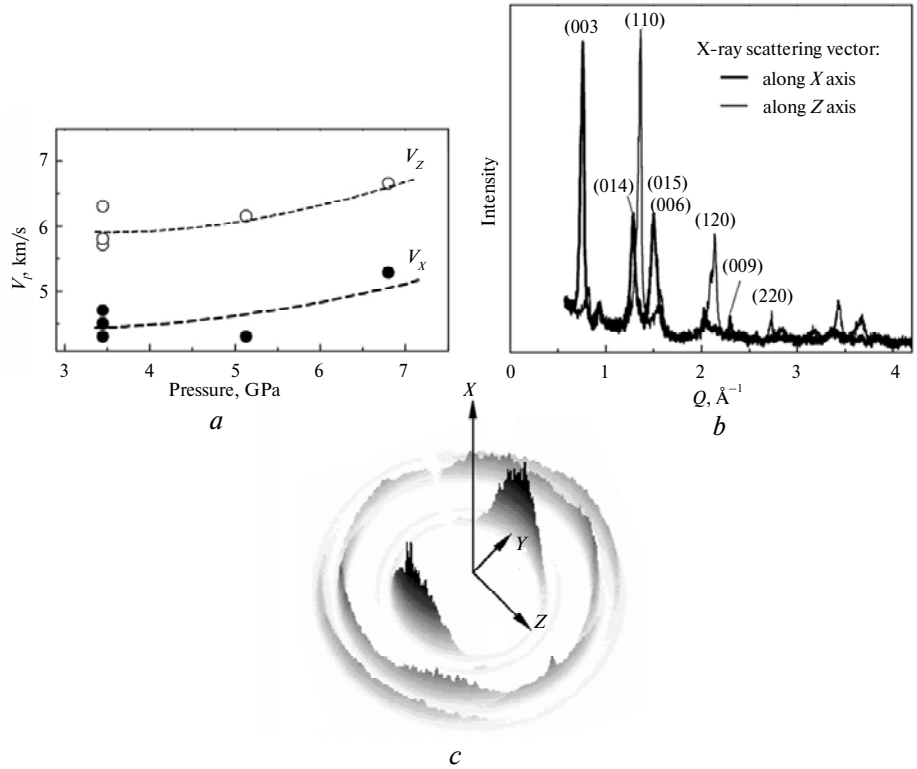

Fig. 17. Anisotropy of the 2D polymerized rhombohedral C_{60} phases revealed by longitudinal ultrasonic velocities plotted as a function of the synthesis pressure (*a*), X-ray diffraction patterns (with the subtracted middle lines) recorded in reflection mode for different geometries of the scattering vector (*b*), and 3D plot of intensity from the 2D diffraction image obtained in transmission mode with the X-ray beam along the *X* axis (*c*). The *Z* axis corresponds to the pressure chambers load direction (additional uniaxial pressure component).

Summarizing this section, one can conclude that any study of physical properties of carbon materials obtained from C_{60} should take into account the prehistory of synthesized samples, such as the pressure–temperature paths, kinetic parameters of experiment, and nonhydrostatic component of the pressure in pressure-transmitting medium.

11. CONCLUSIONS

Finally, the following main trends can be recognized in the structural transformations of C_{60} under high pressure: (i) C_{60} fullerite under high pressure and temperature transforms to a more stable graphite or diamond through the intermediate polymolecular and disordered phases, (ii) an increase in the temperature acting on C_{60} leads eventually to the irreversible destruction of the molecular structure, and (iii) an increase in pressure on heating C_{60} leads to an increase in the density of the synthesized phases and in the mean coordination number of carbon atoms (in the interval from 3 to 4). In this sense the behavior of fullerites is similar to the high pressure behavior of nanotubes [120] or cold compressed graphite [121].

The data on mechanical properties of pressure-synthesized phases provide the key information for potential ways of application of C_{60}-based materials. One can select three groups of novel C_{60}-based carbon materials with properties promising for future applications: (i) moderate pressure (0.1–8 GPa) disordered sp^2-based carbon phases; (ii) superhard diamond-based nanocomposites (ceramics), synthesized at pressures ≥ 12 GPa and high temperatures; (iii) 3D polymerized C_{60}-based materials (pressures higher than 9 GPa and moderate temperatures).

The low-pressure disordered sp^2-based carbon phases have an interesting combination of high hardness up to 30 GPa and a high elastic recovery and low density (1.6 to 2.4 g/cm^3). There are two technological advantages in this material. The pressures necessary for the synthesis of these phases are available for operating large-volume high-pressure devices. Therefore, the synthesis of specimens with a large size and controllable shape is potentially accessible using the high-pressure techniques.

The superhard diamond-based high-pressure disordered phases can have mechanical properties, including hardness and fracture toughness, comparable to or even exceeding those of the best specimens of natural diamonds, due to the nanocomposite structure of these materials. Recent study of nanopolycrystalline diamonds indeed demonstrates their extraordinary wear resistance and hardness [122]. The 3D-polymerized C_{60}-based materials have a unique combination of high hardness and high plasticity. All high-pressure C_{60}-based materials can be applied in future high-pressure techniques. In particular, we proposed in [28] the use of the 3D polymerized phases as a material for gaskets employed in experiments with the generation of extremely high pressures.

We are grateful to prof. Stishov and Popova, for helpful discussions. The work has been supported by the RFBR (11-02-00303, 11-02-00341 and 10-02-01407) and by the Programs of the Presidium of RAS.

Представлено огляд структурних і механічних властивостей твердих вуглецевих фаз, синтезованих з фулерита C_{60} під тиском. Щільність і наноструктура є ключовими параметрами, що визначають механічні властивості твердих фаз вуглецю. Пропонується версія діаграми перетворення при високому тиску C_{60} (розроблена до 20 ГПа), виділено три області формування твердих фаз вуглецю, яким відповідають: 1) невпорядковані sp^2-типу атомні структури при помірних тисках і високих (> 1100 K) температурах, 2) тривимірно полімеризовані C_{60} структури при помірних температурах і високих (> 8 ГПа) тисках, 3) аморфні і нанокомпозитні фази на основі sp^3 при високих

тисках і температурах. Перша область може бути, в свою чергу, розділена на два підрозділи з різними особливостями sp^2-структури і властивостей: область низького (0.1–2 ГПа) і високого (2–8 ГПа) тиску. Температура може бути визнана фактором, відповідальним за формування наноструктур завдяки частковому руйнуванню молекулярних фаз, тоді як тиск є чинником, що стимулює формування жорстких полімеризованих структур, які складаються з ковалентно зв'язаних молекул C_{60}, а поєднання обох факторів приводить до утворення фаз на основі атомів з домінуючим sp^3-зв'язком.

***Ключові слова**: вуглець, алмаз, фулерит C_{60}, наноструктури, полімеризації, надтверді фази.*

Представлен обзор структурных и механических свойств твердых углеродных фаз, синтезированных из фуллерита C_{60} под давлением. Плотность и наноструктура являются ключевыми параметрами, определяющими механические свойства твердых фаз углерода. Предлагается версия диаграммы превращения при высоком давлении C_{60} (разработана до 20 ГПа), выделены три области формирования твердых фаз углерода, которым соответствуют: 1) неупорядоченные sp^2-типа атомные структуры при умеренных давлениях и высоких (> 1100 K) температурах, 2) трехмерно полимеризованные C_{60} структуры при умеренных температурах и высоких (> 8 ГПа) давлениях, 3) аморфные и нанокомпозитные фазы на основе sp^3 при высоких давлениях и температурах. Первая область может быть, в свою очередь, разделена на два подраздела с различными особенностями sp^2-структуры и свойств: область низкого (0.1–2 ГПа) и высокого (2–8 ГПа) давления. Температура может быть признана фактором, ответственным за формирование наноструктур путем частичного разрушения молекулярных фаз, в то время как давление является фактором, стимулирующим формирование жестких полимеризованных структур, состоящих из ковалентно связанных молекул C_{60}, а сочетание обоих факторов приводит к образованию фаз на основе атомов с доминирующей sp^3-связью.

***Ключевые слова**: углерод, алмаз, фуллерит C_{60}, наноструктуры, полимеризации, сверхтвердые фазы.*

1. *Harrison W. A.* Electronic structure and the properties of solids. – San Francisco: Freeman, 1980. – 370 p.
2. *Krätschmer W., Lamb L. D., Fostiropolous K., Huffman D. R.* Solid C_{60}: a new form of carbon // Nature. – 1990. – **347**, N 6291. – P. 354–358.
3. *Brazhkin V. V., Lyapin A. G.* Transformations of C_{60} fullerite under high pressure-high temperature conditions // Physics-Uspekhi. – 1996. – **39**, N 8. – P. 837– 840.
4. *Lyapin A. G.* Mechanical properties of polymerized, amorphous, and nanocrystalline carbon phases prepared from fullerite C_{60} under pressure // Perspectives of Fullerene Nanotechnology / Ed. E. Osawa. – Dordrecht: Kluwer, 2002. – P. 199–216.
5. *Brazhkin V. V., Lyapin A. G., Popova S. V. et al.* Interplay between the structure and properties of new metastable carbon phases obtained under high pressures from fullerite C_{60} and carbyne // JETP Letters. – 2002. – **76**, N 11. – P. 681–692.
6. *Iwasa Y., Arima T., Fleming R. M. et al.* New phases of C_{60} synthesized at high pressure // Science. – 1994. – **264**, N 5165. – P. 1570–1572.
7. *Nunez-Regueiro M., Marques L., Hodeau J.-L. et al.* Polymerized fullerite structures // Phys. Rev. Lett. – 1995. – **74**, N 2. – P. 278–281.
8. *Marques L., Hodeau J.-L., Nunez-Regueiro M., Perroux M.* Pressure and temperature diagram of polymerized fullerite // Phys. Rev. B. – 1996. – **54**, N 18. – P. R12633–R12636.
9. *Davydov V. A., Kashevarova L. S., Rakhmanina A. V. et al.* Identification of the polymerized orthorhombic phase of C_{60} fullerene // JETP Lett. – 1997. – **66**, N 2. – P. 120–125.
10. *Agafonov V., Davydov V. A., Kashevarova L. S. et al.* 'Low-pressure' orthorhombic phase formed from pressure-treated C_{60} // Chem. Phys. Lett. – 1997. – **267**, N 1–2. – P. 193–198.
11. *Davydov V. A., Kashevarova L. S., Rakhmanina A. V. et al.* Tetragonal polymerized phase of C_{60} // Phys. Rev. B. – 1998. – **58**, N 22. – P. 14786–14790.
12. *Davydov V. A., Kashevarova L. S., Rakhmanina A. V. et al.* Spectroscopic study of pressure-polymerized phases of C_{60} // Ibid. – 2000. – **61**, N 18. – P. 11936–11945.
13. *Bennington S. M., Kitamura N., Cain M. G. et al. In situ* diffraction measurement of the polymerization of C_{60} at high temperatures and pressures // J. Phys.: Condens. Matter. – 2000. – **12**, N 28. – P. L451–L456.

14. *Wood R. A., Lewis M. H., West G. et al.* Transmission electron microscopy, electron diffraction and hardness studies of high-pressure and high-temperature treated C_{60} // Ibid. – 2000. – **12**, N 50. – P. 10411–10421.
15. *Meletov K. P., Davydov V. A., Arvanitidis J. et al.* Photo- and pressure-induced transformations in the linear orthorhombic polymer of C_{60} // JETP. – 2008. – **107**, N 4. – P. 620–631.
16. *Meletov K. P., Kourouklis G. A., Arvanitidis J. et al.* Pressure-induced transformation and phonon modes of the two-dimensional rhombohedral polymer of C_{60}: a Raman spectroscopic study // Phys. Rev. B. – 2003. – **68**, N 9, art. 094103.
17. *Kozlov M. E., Hirabayashi M., Nozaki, K. et al.* Transformation of C_{60} fullerenes into a superhard form of carbon at moderate pressure // Appl. Phys. Lett. – 1995. – **66**, N 10. – P. 1199–1201.
18. *Lyapin A. G., Brazhkin V. V., Gromnitskaya E. L. et al.* Hardening of fullerite C_{60} during temperature-induced polymerization and amorphization under pressure // Ibid. – 2000. – **76**, N 6. – P. 712–714.
19. *Lasjaunias J. C., Saint-Paul M., Bilušić A. et al.* Acoustic and thermal transport properties of hard carbon formed from C_{60} fullerene // Phys. Rev. B. – 2002. – **66**, N 1, art. 014302.
20. *Blank V. D., Denisov V. N., Ivlev A. N. et al.* Hard disordered phases produced at high-pressure–high-temperature treatment of C_{60} // Carbon. – 1998. – **36**, N 9. – P. 1263–1267.
21. *Brazhkin V. V., Solozhenko V. L., Bugakov V. I. et al.* Bulk nanostructured carbon phases prepared from C_{60}: approaching the "ideal" hardness // J. Phys.: Condens. Matter. – 2007. – **19**, N 23, art. 236209.
22. *Brazhkin V. V., Lyapin A. G., Antonov Yu. V. et al.* Amorphization of fullerite (C_{60}) at high pressures // JETP Lett. – 1995. – **62**, N 4. – P. 350–355.
23. *Blank V. D., Buga S. G., Serebryanaya N. R. et al.* Ultrahard and superhard carbon phases produced from C_{60} by heating at high pressure: structural and Raman studies // Phys. Lett. A. – 1995. – **205**, N 2–3. – P. 208–216.
24. *Brazhkin V. V., Lyapin A. G., Popova S. V.* Mechanism of three-dimensional polymerization of fullerite C_{60} at high pressures // JETP Lett. – 1996. – **64**, N 11. – P. 802–807.
25. *Blank V. D., Buga S. G., Serebryanaya N. R. et al.* Phase transformations in solid C_{60} at high-pressure-high-temperature treatment and the structure of 3D polymerized fullerites // Phys. Lett. A. – 1996. – **220**, N 1–3. – P. 149–157.
26. *Brazhkin V. V., Lyapin A. G., Popova S. V. et al.* Metastable crystalline and amorphous carbon phases obtained from fullerite C_{60} by high-pressure–high-temperature treatment // Phys. Rev. B. – 1997. – **56**, N 18. – P. 11465–11471.
27. *Lyapin A. G., Brazhkin V. V., Lyapin S. G., Popova S. V.* Three-dimensional polymerization of fullerite C_{60} under high pressure // Rev. High Pressure Sci. Technol. – 1998. – **7**, N 1. – P. 811–813.
28. *Brazhkin V. V., Lyapin A. G., Popova S. V. et al.* Mechanical properties of the 3D polymerized, sp^2–sp^3 amorphous, and diamond-plus-graphite nanocomposite carbon phases prepared from C_{60} under high pressure // J. Appl. Phys. – 1998. – **84**, N 1. – P. 219–226.
29. *Brazhkin V. V., Lyapin A. G.* Comment on "new metallic crystalline carbon: three dimensionally polymerized C_{60} fullerite" // Phys. Rev. Lett. – 2000. – **85**, N 26. – P. 5671–5671.
30. *Horikawa T., Suito K., Kobayashi M., Onodera A.* Time-resolved X-ray diffraction study of C_{60} at high pressure and temperature // Phys. Lett. A. – 2001. – **287**, N 1–2. – P. 143–151.
31. *Talyzin A. V., Dubrovinsky L.S., Oden M. et al. In situ* x-ray diffraction study of C_{60} polymerization at high pressure and temperature // Phys. Rev. B. – 2002. – **66**, N 16, art. 165409.
32. *Wood R. A., Lewis M. H., Bennington S. M. et al.* In situ x-ray diffraction studies of three-dimensional C_{60} polymers // J. Phys.: Condens. Matter. – 2002. – **14**, N 45. – P. 11615–11621.
33. *Mezouar M., Marques L., Hodeau J.-L. et al.* Equation of state of an anisotropic three-dimensional C_{60} polymer: the most stable form of fullerene // Phys. Rev. B. – 2003. – **68**, N 19, art. 193414.
34. *Yamanaka Sh., Kubo A., K. Inamuru K. et al.* Electron conductive three-dimensional polymer of cuboidal C_{60} // Phys. Rev. Lett. – 2006. – **96**, N 7, art. 076602.
35. *Talyzin A. V., Dubrovinsky L. S. In situ* Raman study of path-dependent C_{60} isothermal compression up to 32 polymerization: GPa at 800 K // Phys. Rev. B. – 2003. – **68**, N 23, art. 233207.
36. *Talyzin A. V., Dubrovinsky L. S.* In situ Raman study of C_{60} polymerization during isothermal pressurizing at 800 K // J. Phys.: Condens. Matter. – 2004. – **16**, N 6. – P. 757–772.

37. *Talyzin A. V., Langenhorst F., Dubrovinskaia N. et al.* Structural characterization of the hard fullerite phase obtained at 13 GPa and 830 K // Phys. Rev. B. – 2005. – **71**, N 11, art. 115424.
38. *Hirai H., Kondo K., Yoshizava N., Shiraishi M.* Amorphous diamond from C_{60} fullerene // Appl. Phys. Lett. – 1994. – **64**, N 14. – P. 1797–1799.
39. *Hirai H., Tabira Y., Kondo K. et al.* Radial distribution function of a new form of amorphous diamond shock induced from C_{60} fullerene // Phys. Rev. B. – 1995. – **52**, N 9. – P. 6162–6165.
40. *Brazhkin V. V., Lyapin A. G., Voloshin R. N. et al.* Mechanism of the formation of a diamond nanocomposite during transformations of C_{60} fullerite at high pressure // JETP Lett. – 1999. – **69**, N 11. – P. 869–875.
41. *Irifune T., Kurio A., Sukamoto Sh. et al.* Ultrahard polycrystalline diamond from graphite // Nature. – 2003. – **421**, N 6923. – P. 599–600.
42. *Sumiya H., Yusa H., Inoue T. et al.* Conditions and mechanism of formation of nano-polycrystalline diamonds on direct transformation from graphite and non-graphitic carbon at high pressure and temperature // High Press. Res. – 2006. – **26**, N 2. – P. 63–69.
43. *Sundqvist B.* Fullerenes under high pressures // Adv. Phys. – 1999. – **48**, N 1. – P. 1–134.
44. *Sundqvist B.* Buckyballs under pressure // Phys. Stat. Sol. (b). – 2001. – **223**, N 1. – P. 469–477.
45. *Makarova T. L.* Electrical and Optical Properties of Pristine and Polymerized Fullerenes // Semiconductors (St. Petersburg). – 2001. – **35**, N 3. – P. 243–278.
46. *Sneddon I. N.* Boussinesq's problem for a rigid cone // Math. Proc. Cambridge Phil. Soc. – 1948. – **44**, N 4. – P. 492–507; The relation between load and penetration in the axisymmetric boussinesq problem for a punch of arbitrary profile // Int. J. Eng. Sci. – 1965. – **3**, N 1. – P. 47–57.
47. *Gong J., Wu J., and Guang Z.* Examination of the indentation size effect in low-load vickers hardness testing of ceramics // J. Europ. Ceram. Soc. – 1999. – **19**, N 15. – P. 2625–2631.
48. *Serebryanaya N. R., Blank V. D., Ivdenko V. A., Chernozatonskii L. A.* Pressure-induced superhard phase of C_{60} // Solid State Comm. – 2001. – **118**, N 4. – P. 183–187.
49. *Lyapin A. G., Mukhamadiarov V. V., Brazhkin V. V. et al.* Structural and elastic anisotropy of carbon phases prepared from fullerite C_{60} // Appl. Phys. Lett. – 2003. – **83**, N 19. – P. 3903–3905.
50. *Brazhkin V. V., Lyapin A. G., Hemley R. J.* Harder than diamond: dreams and reality // Phil. Mag. A. – 2002. – **82**, N 2. – P. 231–253.
51. *Thorpe M. F.* Continuous deformations in random networks // J. Non-Cryst. Sol. – 1983. – **57**, N 3. – P. 355–370.
52. *Kelires P. C.* Intrinsic stress and stiffness variations in amorphous carbon // Diamond Relat. Mater. – 2001. – **10**, N 2. – P. 139–144.
53. *Tai W. P., Watanabe T.* Preparation and mechanical properties of Al_2O_3 reinforced by submicrometer Co particles // J. Mat. Sci. – 1998. – **33**, N 24. – P. 5795–5801.
54. *Yip S.* The strongest size // Nature. – 1998. – **391**, N 6667. – P. 532–533.
55. *Jacobsen K. W., Schiotz J.* Nanoscale plasticity // Nature Mater. – 2002. – **1**, N 1. – P. 15–16.
56. *Yusa H.* Nanocrystalline diamond directly transformed from carbon nanotubes under high pressure // Diamond Relat. Mater. – 2002. – **11**, N 1. – P. 87–91.
57. *Evans A. R., Wilshaw T. R.* Quasi-static solid particle damage in brittle solids. I. Observations analysis and implications // Acta Metall. – 1976. – **24**, N 10. – P. 939–956.
58. *Dworkin A., Szwarc H., Davydov V. A. et al.* Thermal studies of C_{60} transformed by temperature and pressure treatments // Carbon. – 1997. – **35**, N 6. – P. 745–747.
59. *Davydov V. A., Kashevarova L. S., Rakhmanina A. V. et al.* Particularities of C_{60} transformations at 1.5 GPa // J. Phys. Chem. B. – 1999. – **103**, N 11. – P. 1800–1804.
60. *Kondrin M. N., Lyapin A. G., Brazhkin V. V., Popova S. V.* The influence of dimerization on the oorientational phase transition in the C_{60} fullerite // Phys. Solid State (St. Petersburg). – 2002. – **44**, N 3. – P. 447–449.
61. *Brazhkin V. V., Lyapin A. G.* Hard carbon phases prepared from fullerite C_{60} under high pressure // New Diamond Frontier Carbon Technol. – 2004. – **14**, N 5. – P. 259–278.
62. *Sundqvist B.* Comment on "Pressure and temperature diagram of polymerized fullerite" // Phys. Rev. B. – 1998. – **57**, N 5. – P. 3164–3165.
63. *Blank V. D., Buga S. G., Dubitsky G. A. et al.* High-pressure polymerized phases of C_{60} // Carbon. – 1998. – **36**, N 4. – P. 319–343.
64. *Duclos S. J., Brister K., Haddon R. C. et al.* Effects of pressure and stress on C_{60} fullerite to 20 GPa // Nature. – 1991. – **351**, N 6325. – P. 380–382.

65. *Nunez-Regueiro M., Monceau P., Rassat A. et al.* Absence of a metallic phase at high pressures in C_{60} // Ibid. – 1991. – **354**, N 6351. – P. 289–291.
66. *Yoo C. S., Nellis W. J.* Phase transformations in carbon fullerenes at high shock pressures // Science. – 1991. – **254**, N 5037. – P. 1489–1491.
67. *Nunez-Regueiro M., Monceau P., Hodeau J.-L.* Crushing C_{60} to diamond at room temperature // Nature. – 1992. – **355**, N 6357. – P. 237–239.
68. *Nunez-Regueiro M., Abello L., Lucazeau G., and Hodeau J.-L.* Diamond from fullerenes: evidence from Raman measurements // Phys. Rev. B. – 1992. – **46**, N 15. – P. 9903–9905.
69. *Snoke D. W., Raptis Y. S., Syassen K.* Vibrational modes, optical excitations, and phase transition of solid C_{60} at high pressures // Ibid. – 1992. – **45**, N 24. – P. 14419–14422.
70. *Moshary F., Chen N. H., Silvera I. F. et al.* Gap reduction and the collapse of solid C_{60} to a new phase of carbon under pressure // Phys. Rev. Lett. – 1992. – **69**, N 3. – P. 466–469.
71. *Kosowsky S.D., Hsu C.-H., Chen N.H. et al.* X-ray study of pressure-collapsed fullerite // Phys. Rev. B. – 1993. – **48**, N 11. – P. 8474–8475.
72. *Yoo C. S., Nellis W. J.* Phase transition from C_{60} molecules to strongly interacting C_{60} agglomerates at hydrostatic high pressures // Chem. Phys. Lett. – 1992. – **198**, N 3–4. – P. 379–382.
73. *Hodeau J.-L., Tonnerre J. M., Bouchet-Fabre B. et al.* High-pressure transformations of C_{60} to diamond and sp^3 phases at room temperature and to sp^2 phases at high temperature // Phys. Rev. B. – 1994. – **50**, N 14. – P. 10311–10314.
74. *Yoo C. S., Nellis W. J., Satler M. L., Musket R. G.* Diamondlike metastable carbon phases from shock-compressed C_{60} films // Appl. Phys. Lett. – 1992. – **61**, N 3. – P. 273–275.
75. *Matsumuro A., Takada Y., Takahashi Y. et al.* Mechanical properties of C_{60} bulk materials synthesized at high pressure // Rev. High Pressure Sci. Technol. – 1998. – **7**, N 1. – P. 823–825.
76. *Blank V. D., Kulnitskiy B. A., Tatyanin Ye. V.* Structural studies of high pressure phases of C_{60} // Phys. Lett. A. – 1995. – **204**, N 2. – P. 151–154.
77. *Marques L., Mezouar M., Hodeau J.-L. et al.* "Debye-Scherrer ellipses" from 3D fullerene polymers: an anisotropic pressure memory signature // Science. – 1999. – **283**, N 5408. – P. 1720–1723.
78. *Okada S., Saito S., Oshiyama A.* New metallic crystalline carbon: three dimensionally polymerized C_{60} fullerite // Phys. Rev. Lett. – 1999. – **83**, N 10. – P. 1986–1989.
79. *Burgos E., Halac E., Weht R. et al.* New superhard phases for three-dimensional C_{60}-based fullerites // Ibid. – 2000. – **85**, N 11. – P. 2328–2331.
80. *Perottoni C. A., da Jornada J. A. H.* First-principles calculation of the structure and elastic properties of a 3D-polymerized fullerite // Phys. Rev. B. – 2002. – **65**, N 22, art. 224208.
81. *Yamagami Y., Saito S.* Polymerized sp^2–sp^3 hybrid metallic phase of C_{60} as obtained via constant-pressure molecular dynamics // Ibid. – 2009. – **79**, N 4, art. 045425.
82. *Yang J., Tse J. S.* First-principles investigation on the geometry and electronic structure of the three-dimensional cuboidal C_{60} polymer // J. Chem. Phys. – 2007. – **127**, N 13, art. 134906.
83. *Berber S., Osawa E., Tománek D.* Rigid crystalline phases of polymerized fullerenes // Phys. Rev. B. – 2004. – **70**, N 8, art. 085417.
84. *Zipoli F., Bernasconi M.* First principles study of three-dimensional polymers of C_{60}: structure, electronic properties, and Raman spectra // Ibid. – 2008. – **77**, N 11, art. 115432.
85. *Talyzin A. V., Dubrovinsky L. S., Jansson U. In situ* Raman study of C_{60} thin films at high pressures // Ibid. – 2001. – **64**, N 11, art. 113408.
86. *Ivanovskaya V. V., Ivanovskii A. L.* Simulation of novel superhard carbon materials based on fullerenes and nanotubes // J. Superhard Mat. – 2010. – **32**, N 2. – P. 67–87.
87. *Chi D. H., Iwasa Y., Takano T. et al.* Bond switching from two- to three-dimensional polymers of C_{60} at high pressure // Phys. Rev. B. – 2003. – **68**, N 15, art. 153402.
88. *Goze C., Rachdi F., Hajji L. et al.* High-resolution ^{13}C NMR studies of high-pressure-polymerized C_{60}: Evidence for the 2+2. cycloaddition structure in the rhombohedral two-dimensional C_{60} polymer // Ibid. – 1996. – **54**, N 6. – P. R3676–R3678.
89. *He H., Thorpe M. F.* Elastic properties of glasses // Phys. Rev. Lett. – 1985. – **54**, N 19.– P. 2107–2110.
90. *Blank V. D., Tatyanin Ye. V., Kulnitskiy B. A.* New structure after thermobaric treatment of solid C_{60} // Phys. Lett. A. – 1997. – **225**, N 1–3. – P. 121–126.
91. *Ferrari A. C., Robertson J.* Interpretation of Raman spectra of disordered and amorphous carbon // Phys. Rev B. – 2000. – **61**, N 20. – P. 14095–14107.

92. *Townsend S. J., Lenosky T. J., Muller D. A. et al.* Negatively curved graphitic sheet model of amorphous carbon // Phys. Rev. Lett. – 1992. – **69**, N 6. – P. 921–924.
93. *Donadio D., Colombo L., Benedek G.* Elastic moduli of nanostructured carbon films // Phys. Rev. B. – 2004. – **70**, N 19, art. 195419.
94. *Alexandrou I., Scheibe H.-J., Kiely C. J. et al.* Carbon films with an sp^2 network structure. Ibid. – 1999. – **60**, N 15. – P. 10903–10907.
95. *Barnett S., Madan A.* Superhard superlattices // Physics World. – 1998. – **11**, N 1. – P. 45–48.
96. *Weiler M., Sattel S., Giessen T. et al.* Preparation and properties of highly tetrahedral hydrogenated amorphous carbon // Phys. Rev. B. – 1996. – **53**, N 3. – P. 1594–1608.
97. *Onodera A., Irie Y., Higash, K. et al.* Graphitization of amorphous carbon at high pressures to 15 GPa // J. Appl. Phys. – 1991. – **69**, N 4. – P. 2611–2617.
98. *Clerc D. G., Ledbetter H. M.* Mechanical hardness: a semiempirical theory based on screened electrostatics and elastic shear // J. Phys. Chem. Solids. – 1998. – **59**, N 6–7. – P. 1071–1095.
99. *Teter D. M.* Computational alchemy: the search for new superhard materials // MRS Bulletin. – 1998. – **23**, N 1. – P. 22–27.
100. *Blank V. D., Serebryanaya N. R., Dubitsky G. A. et al.* Polymerization and phase diagram of solid C_{70} after high-pressure-high-temperature treatment // Phys. Lett. A. – 1998. – **248**, N 5–6. – P. 415–422.
101. *Patterson J. R., Catledge S. A., Vohra Y. K. et al.* Electrical and mechanical properties of C_{70} fullerene and graphite under high pressures studied using designer diamond anvils // Phys. Rev. Lett. – 2000. – **85**, N 25. – P. 5364–5367.
102. *Brazhkin V. V., Lyapin A. G., Popova, S. V. et al.* Mechanical properties of the superhard polymeric and disordered phases prepared from C_{60}, C_{70}, and C_{2N} under high pressure // Rev. High Pressure Sci. Technol. – 1998. – **7**, N 1. – P. 989–991.
103. *Sjöström H., Stafström S., Boman M., Sundgren J.-E.* Superhard and elastic carbon nitride thin films having fullerenelike microstructure // Phys. Rev. Lett. – 1995. – **75**, N 7. – P. 1336–1339.
104. *Brazhkin V. V., Glazov A. G., Mukhamadiarov V. V. et al.* Elastic properties of carbon phases obtained from C_{60} under pressure: the first example of anisotropic disordered carbon solid // J. Phys.: Condens. Matter. – 2002. – **14**, N 44. – P. 10911–10915.
105. *Mukhamadiarov V. V., Lyapin A. G., Popova S. V. et al.* Directional anisotropy in carbon phases prepared from fullerite C_{60} under high pressures // High Press. Res. – 2003. – **23**, N 3. – P. 275–279.
106. *Manghnani M. H., Tkachev S., Zinin P. V. et al.* Elastic properties of superhard amorphous carbon pressure-synthesized from C_{60} by surface Brillouin scattering // Phys. Rev. B. – 2001. – **64**, N 12, art. 121403(R).
107. *Kelires P. C.* Elastic properties of amorphous carbon networks // Phys. Rev. Lett. – 1994. – **73**, N 18. – P. 2460–2463.
108. *Liu A. Y., Cohen M. L., Hass K. C., Tamor M. A.* Structural properties of a three-dimensional all-sp^2 phase of carbon // Phys. Rev. B. – 1991. – **43**, N 8. – P. 6742–6745.
109. *Jungnickel G., Sitch P. K., Frauenheim Th. et al.* Nitrogen doping in purely sp^2 bonded forms of carbon // Ibid. – 1998. – **57**, N 2. – P. R661–R665.
110. *Côté M., Grossman J. C., Cohen M. L., Louie S. G.* Theoretical study of a three-dimensional all-sp^2 structure // Ibid. – 1998. – **58**, N 2. – P. 664–668.
111. *Rosato V., Celino M., Benedek G., Gaito S.* Thermodynamic behavior of the carbon schwarzite fcc $(C_{36})_2$ // Ibid. – 1999. – **60**, N 24. – P. 16928–16933.
112. *Mailhiot C., McMahan A. K.* Atmospheric-pressure stability of energetic phases of carbon // Ibid. – 1991. – **44**, N 21. – P. 11578–11591.
113. *Lyapin A. G., Brazhkin V. V.* Correlations between the physical properties of the carbon phases obtained at a high pressure from C_{60} fullerite // Phys. Solid State (St. Petersburg). – 2002. – **44**, N 3. – P. 405–409.
114. *Meletov K. P., Kourouklis G. A., Arvanitidis et al.* J. Pressure-induced transformation and phonon modes of the two-dimensional rhombohedral polymer of C_{60}: a Raman spectroscopic study // Phys. Rev. B. – 2003. – **68**, N 9, art. 094103.
115. *Marques L., Mezouar M., Hodeau J.-L., Nunez-Regueiro M.* Imprinting of anisotropic stress during C_{60} high-pressure/high-temperature polymerization process // Ibid. – 2002. – **65**, N 10, art. 100101(R).
116. *Prokhorov V. M., Blank V. D., Buga S. G., Levin V. M.* Scanning acoustic microscopy study of superhard C_{60}-based polymerized fullerites // Synthetic Metals. – 1999. – **103**, N 1–3. – P. 2439–2442.

117. *Levin V. M., Blank V. D., Prokhorov V. M. et al.* Elastic modules of solid C_{60}: measurement and relationship with nanostructure // J. Phys. Chem. Sol. – 2000. – **61**, N 7. – P. 1017–1024.
118. *Tat'yanin E. V., Lyapin A. G., Mukhamadiarov V. V. et al.* Mechanism of formation of the superhard disordered graphite-like phase from fullerite C_{60} under pressure // J. Phys.: Cond. Mat. – 2005. – **17**, N 2. – P. 249– 256.
119. *Alvarez-Murga M., Bleuet P., Marques L. et al.* Microstructural mapping of C_{60} phase transformation into disordered graphite at high pressure, using X-ray diffraction microtomography // J. Appl. Cryst. – 2011. – **44**, N 1. – P. 163–171.
120. *Zhao Z. S., Zhou X.-F., Hu M. et al.* High-pressure behaviors of carbon nanotubes // J. Superhard Mater. – 2012. – **34**, N 6. – P. 371–385.
121. *Boulfelfel S. E., Zhu Q., Oganov A. R.* Novel sp^3-forms of carbon predicted by evolutionary metadynamics and analysis of their synthesizability using transition path sampling // Ibid. – 2012. – **34**, N 6. – P. 350–359.
122. *Kurio A., Tanaka Y., Sumiya H. et al.* Wear resistance of nano-polycrystalline diamond with various hexagonal diamond contents // Ibid. – 2012. – **34**, N 6. – P. 343–349.

Institute for High Pressure Physics Received 21.09.12